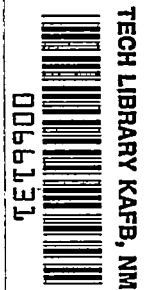


6186

NACA TN 3015

TN
3015
a.1

NATIONAL ADVISORY COMMITTEE FOR AERONAUTICS

TECHNICAL NOTE 3015

LOAN COPY: RETURN TO
AFWL TECHNICAL LIBRARY
KIRTLAND AFB, N. M.

AN EXPERIMENTAL INVESTIGATION OF SECONDARY FLOW
IN AN ACCELERATING, RECTANGULAR ELBOW
WITH 90° OF TURNING

By John D. Stanitz, Walter M. Osborn, and John Mizisin

Lewis Flight Propulsion Laboratory
Cleveland, Ohio



Washington
October 1953

AFMDC
TECHNICAL LIBRARY
APL 2011

NATIONAL ADVISORY COMMITTEE FOR AERONAUTICS

TECHNICAL NOTE 3015

AN EXPERIMENTAL INVESTIGATION OF SECONDARY FLOW IN AN ACCELERATING,
RECTANGULAR ELBOW WITH 90° OF TURNING

By John D. Stanitz, Walter M. Osborn, and John Mizisin

SUMMARY

Secondary flow tests were conducted on an accelerating elbow with 90° of turning designed for prescribed velocities that eliminate boundary-layer separation by avoiding local decelerations along the walls. Secondary flows were investigated for six boundary-layer thicknesses generated on the plane walls of the elbow by spoilers upstream of the elbow inlet. For each spoiler size, total-pressure surveys at the inlet and exit planes of the elbow and complete spanwise static-pressure distributions on the pressure and suction surfaces of the elbow were obtained. The test results were analyzed from continuity and momentum considerations in an effort to correlate the secondary flows at the exit with the inlet flow conditions and the measured wall-static-pressure distributions.

The passage vortex associated with secondary flows appears to be near the suction surface and away from the plane wall of the elbow at the exit and does not have appreciable spanwise motion as it moves downstream from the elbow exit. As the spoiler size increases, the boundary-layer form changes and a rather sudden difference in the secondary flow occurs, perhaps associated with the reduced importance of viscous effects in thick boundary layers. It is suggested that the strength of the secondary vortices is small and that the energy of secondary flows is small.

INTRODUCTION

Secondary flow occurs in fluids with curved streamlines and with total-pressure gradients normal to the plane of the velocity vector and the radius of streamline curvature. Secondary flow is defined as that motion of the fluid associated with the component of vorticity parallel to the direction of flow. As a first approximation, this flow is more simply defined as that motion of the fluid associated with the velocity components normal to the potential flow direction (irrotational flow, which has constant total pressure). It is, for all practical purposes, the motion of boundary layer and other low-energy flow in directions different from the main flow.

3005

CY-1

These secondary flows occur in compressors, turbines, elbows, and other flow channels where the fluid is turned and where, as a result of viscous dissipation, the total pressure varies. Consider, for example, the flow through an elbow with a rectangular cross section. For real, viscous fluids the velocity distribution upstream of the elbow is non-uniform so that the total pressure varies and the fluid motion is rotational. Such rotational, or shear, flows can develop both normal to and in the plane of the elbow. If the shear flow develops in the plane of the elbow so that the vorticity vectors are normal to the plane, the shear flow remains two-dimensional and in the plane of the elbow. This type of flow has been investigated analytically in reference 1. If the shear flow, and therefore the total-pressure variation, develops normal to the plane of the elbow so that the upstream vorticity vectors are parallel to the plane, three-dimensional secondary flows develop in the elbow. The physical mechanism of secondary flow is readily visualized for the case of a relatively thin boundary layer through which, according to boundary-layer theory, the static-pressure gradients set up by the main flow (which is potential) persist. Because the low-velocity boundary layer does not require the pressure gradients imposed on it in order to turn with a radius of curvature equal to that of the main flow, the boundary layer moves in directions different from the direction of the main flow, and the motion associated with these differences is called secondary flow.

Secondary flows influence the performance of compressors, turbines, elbows, and other channels in several ways: These flows (1) transfer low-energy fluid to regions (surfaces) of decelerating flow where separation may result; (2) in compressors and turbines, influence the blade setting angles for minimum energy losses; (3) affect the angle of attack in subsequent blade rows and influence the efficiency of addition to or extraction from the energy of the fluid in compressors and turbines; and (4) involve kinetic energies that are eventually lost by viscous dissipation. Secondary flows have therefore been the subject of many experimental investigations (refs. 2 to 8, for example) and several analytical investigations (refs. 9 to 11, for example).

In previous experimental investigations, especially those on elbows, the mechanism of secondary flow has been complicated by the presence of separated boundary layers that result from local decelerations along the flow surfaces. In order to avoid this complication and therefore to obtain better experimental data for secondary flow studies, an elbow has been designed (ref. 12) for a prescribed velocity distribution that decelerates nowhere along the elbow walls and therefore avoids boundary-layer separation. The results of secondary flow tests on this elbow are

reported herein. Because secondary flows ultimately develop from the static pressures on the elbow walls, the main object of these tests was to measure the static-pressure distributions on the inner (suction) and outer (pressure) walls of the elbow and to correlate these pressure distributions with the inlet and exit flow conditions of the elbow. These tests were conducted for six boundary-layer thicknesses generated on the plane walls of the elbow by spoilers upstream of the inlet. The work was carried out at the NACA Lewis laboratory.

APPARATUS AND INSTRUMENTATION

As indicated in the line drawing of figure 1, the 90° elbow is attached to a short tunnel of straight parallel walls that is mounted on a rounded approach at the top of the flow test tank. A constant-area duct 6 inches long from which the air is discharged into the test cell is attached at the exit of the elbow. This apparatus and the instrumentation are now described.

Description of Apparatus

Flow test tank. - The flow test tank is approximately 5 feet in diameter. Other dimensions of the tank and piping are given in figure 1. The tank contains a honeycomb of square cells (2 by 2 in.) 8 inches deep. Three screens were placed immediately upstream of the honeycomb in order to reduce turbulence - one 28X30 mesh and two 40X60 mesh, with the mesh oriented 90° apart. The tank pressure, and therefore the flow rate, is controlled by a valve upstream of the tank. The profile of the rounded approach, shown in figure 1, is elliptical.

Tunnel and spoilers. - The tunnel length (24 in.) is short in order to provide (in the absence of spoilers) a relatively thin boundary layer at the inlet to the elbow. The cross section of the tunnel normal to the direction of flow is 11.92 inches wide by 16.50 inches deep.

In order to provide various thicknesses of boundary layer, or shear flow, on the plane walls of the elbow at the inlet, spoilers that projected from both plane walls into the air stream were located at the junction between the tank and the tunnel (fig. 1). The spoilers were made of 1/16-inch perforated sheet metal with 1/8-inch diameter holes centered to form equilateral triangles (fig. 2) and spaced to give a solidity (ratio of metal area to total area) of 0.60. Six spoiler sizes, projecting into the air stream from 0 to 2.5 inches in increments of 0.5

inch, were used in the tests. Spanwise total-pressure surveys were taken at the elbow inlet (tunnel exit) at the center line of the passage for the six spoiler sizes. Surveys at various positions between the suction and pressure surfaces indicated that the total-pressure profiles were the same as those at the center line of the passage (midway between the pressure and suction surfaces). The resulting boundary-layer velocity profiles, obtained from total-pressure surveys, at the elbow inlet for the six spoiler sizes are given in figure 3 as a function of spanwise distance z (normal to the plane walls of the elbow, see fig. 1) expressed as a ratio (z/w) of the elbow span w (fig. 1). (All symbols are defined in the appendix.) The velocity q is expressed as a ratio (q/q_{\max}) of the maximum velocity q_{\max} in the main flow outside the boundary layer. These profiles were obtained for a tank gage pressure of 20 inches of water, with the elbow removed, and the profiles are assumed to be the same for other values of q_{\max} .

In order to determine the stability of the inlet velocity profiles, profiles were also measured at distances of 2, 6, 12, and 18 inches upstream of the elbow inlet. These profiles are shown for spoiler sizes of 0.5, 1.5, and 2.5 inches in figure 4. The plots indicate that the inlet profiles are not entirely stable, but that the rate of change is moderate.

Elbow. - In order to avoid boundary-layer separation, the elbow was designed (ref. 12) assuming incompressible, potential flow for a prescribed velocity distribution that decelerates nowhere along the pressure (outer) and suction (inner) walls (fig. 1). The xy -coordinates and the prescribed velocity Q along the elbow profile are given in table I as functions of the velocity potential ϕ , where the xy -coordinates are given in inches, the velocity Q is the local velocity expressed as a ratio of the downstream exit velocity, and, for purposes of this report, ϕ may be considered as a dummy variable along the curved walls of the elbow. (The complete definition of ϕ is given in ref. 12.) The prescribed velocity Q increases from an upstream value of 0.5 to a downstream value of 1.0. For this prescribed velocity distribution the elbow turning angle is 89.36° and the channel width in the elbow plane decreases from an upstream value of 11.92 inches to a downstream value of 5.98 inches. The depth (span, see fig. 1) of the elbow is 16.5 inches and other over-all dimensions are given in figure 1. A plot of the elbow plane, showing the streamlines and velocity potential lines, is given in figure 5, and a photograph of the elbow assembled on the tank is shown in figure 6. The elbow was fabricated from 1/2-inch steel plate and the contours were accurate within ± 0.030 inch. A comparison at mid-span of the prescribed velocity distribution and that obtained experimentally, without spoilers, is given in figure 7 for a range of exit Mach number from 0.2 to 0.8. For a Mach number of 0.2 the agreement between design and test values of Q is good (elbow was designed for zero Mach number, that is, incompressible flow) and, for all Mach numbers, serious deceleration of the flow was avoided. It is concluded that no boundary-layer separation occurred in the elbow.

Instrumentation

Tank. - The total pressure in the main flow was measured by four static taps downstream of the honeycomb in the tank (fig. 1). The total temperature of the air was measured by thermocouples in the tank.

Elbow. - In order to measure the spanwise distribution in static pressure from one plane wall to midspan of the elbow, a total of 242 static taps, each 0.030 inch in diameter, were located on the curved walls of the elbow. These static taps were located on both the pressure and suction surfaces at eleven values of ϕ from -0.50 to 4.50 in equal increments of 0.50. At each value of ϕ on each wall there were eleven static taps located at the following distances from the plane wall of the elbow: $1/8$, $3/8$, $5/8$, $1\frac{1}{8}$, $1\frac{5}{8}$, $2\frac{5}{8}$, $3\frac{5}{8}$, $4\frac{5}{8}$, $5\frac{3}{4}$, 7, and $8\frac{1}{4}$ inches, the last tap being at midspan. (Total-pressure surveys at the exit plane indicated the flow to be symmetrical about midspan.) A number of static taps were also located on the four walls of the tunnel upstream of the elbow and on the short extension downstream of the elbow (as a measure of the uniformity of flow).

Total-pressure surveys were made in the exit plane of the short (6-in.) extension downstream of the elbow. These surveys were made with an unshielded total-pressure rake (0.030-in. outside diam. tubing) aligned with the axis of the exit duct as shown in figure 6.

In regions of secondary flow downstream of the elbow, the flow spirals and therefore is not aligned with the axis of the probe (largest deviation should be associated with the thinnest boundary layer (ref. 10)). A total-pressure survey was therefore made in this region, for one test only (no spoiler), using a Kiel-type probe with a $1/8$ -inch diameter shield, in order to determine possible errors in the unshielded total-pressure readings. A comparison of the total-pressure-loss contours obtained with shielded and unshielded probes in the region of secondary flow downstream of the elbow with no spoiler is shown in figure 8. The similarity of the contours suggests that, for these tests (assuming that the shielded probe gives accurate readings), the use of unshielded probes is justified. In figure 8 the pressure ratio P is dimensionless and is defined by

$$P = \frac{P - P_a}{P_T - P_a} \quad (1)$$

where p is the static pressure and the subscripts a and T refer to atmospheric and tank total conditions, respectively. The tank gage pressure ($P_T - p_a$) in the denominator of equation (1) is related to velocity head at the elbow exit. Thus, from equation (1), the ΔP_t in figure (8) becomes

$$\Delta P_t = P_T - P_t = \frac{P_T - P_t}{P_T - p_a} \quad (1a)$$

where ΔP_t , for incompressible flow, represents the loss in velocity head. The subscript t refers to local total conditions, in which case p becomes p_t in equation (1).

RESULTS AND DISCUSSION

Total-pressure surveys were made at the elbow inlet in order to determine the inlet velocity profiles for six spoiler sizes, including no spoiler. Also, for each spoiler size, complete total-pressure surveys were made in the exit plane of the 6-inch extension downstream of the elbow, at a main-stream exit Mach number of 0.4, in order to obtain from the total-pressure-loss distribution an indication of the secondary flow motion. In addition, for the elbow with no spoiler, total-pressure surveys were made in the exit planes of 12-inch and 18-inch extensions, in order to determine the spanwise motion of the low-energy fluid as it moved downstream. Finally, for each spoiler size, complete spanwise wall-static-pressure distributions on the pressure and suction surfaces were obtained for a tank gage pressure of 20 inches of water. These static-pressure distributions were integrated over the wall area to obtain the net force acting on the fluid passing through the elbow.

Downstream Total-Pressure Distributions

Test results. - Contours of constant total-pressure loss ΔP_t , obtained from plots and cross plots of approximately 600 total-pressure data points covering half the flow field in the exit plane of the 6-inch extension, are given in figure 9 for the six spoiler sizes. (The dashed lines in figures 8 and 9(a) are total-pressure-loss contours for ΔP_t increments of less than 0.05, added to give a more detailed picture of the loss contours.) It is noted in figure 9(a), and in figure 8, that an accumulation of low-energy fluid has occurred on the lower (suction) surface of the elbow at the exit. The center of this accumulation appears to correspond roughly to the center of the passage vortex observed for secondary flows in elbows (ref. 7). It is noted that although

3005 the center of the vortex is a region of high total-pressure loss, it is not the region of highest total-pressure loss (which occurs on the walls). It is also noted that fluid of higher loss is perhaps being entrained by the center of the vortex. (Note, for example, the shape of the ΔP_t contours for 0.40, 0.35, and 0.30 in the vicinity of the vortex.) If the Bernoulli surfaces of constant total pressure (that is, constant total-pressure loss) can be assumed to maintain approximately their identity as the flow passes through the elbow, these surfaces (originally parallel to the elbow plane at the inlet) are seen to be "folded" into the passage vortex. Thus, the motion of the boundary-layer secondary flow can be visualized as a progressive sliding of the Bernoulli surfaces off the elbow plane at the inlet onto the suction surface upstream of the exit, where the Bernoulli surfaces fold up into the passage vortex. (Because, in the absence of viscosity, streamlines must lie on Bernoulli surfaces, this folding action of the Bernoulli surfaces cannot be maintained indefinitely, as smoke studies of the vortex (see fig. 10, for example) indicate that the streamlines wind up into a tight spiral.) The sliding motion of the Bernoulli surfaces off the elbow plane results from the excess pressure gradients imposed on the low-energy fluid of the boundary layer by the main flow. These gradients are such as to force the boundary layer, and therefore the Bernoulli surfaces, toward the suction surface.

It is interesting to note in figure 9 that in the exit plane the passage vortex is near the suction surface and away from the plane wall of the elbow, not in the corner. Total-pressure surveys in the exit planes of 12- and 18-inch extensions indicate (fig. 11) that the center of the vortex apparently does not have appreciable spanwise motion as the vortex proceeds downstream from the elbow exit, at least for the smaller spoiler sizes. This fact is confirmed by the smoke filaments in figure 10.

As the spoiler size, and therefore the inlet boundary-layer thickness on the plane wall, increases, it is evident from figure 9 that the magnitude of the low-energy fluid accumulated on the suction surface at the exit increases. Furthermore, the contours of constant ΔP_t indicate that as the inlet boundary layer thickens the passage vortex tends to lose its identity, becoming more "spread-out" and less localized. In figure 9 there is a sudden change in the ΔP_t contour characteristics as the spoiler size is increased from 0.5 to 1.0 inch. For no spoiler and the 0.5-inch spoiler, the vortices are easily identified and apparently rather tightly wound; for the larger spoilers it becomes more difficult to associate the ΔP_t with a well-defined secondary vortex. It is concluded that, as the inlet boundary-layer thickness on the plane wall increases, a rather sudden difference occurs in the secondary flow pattern, perhaps associated with the reduced importance of viscous effects because of the smaller velocity gradients in thick boundary layers.

Although for the larger spoiler sizes it becomes difficult to identify the vortex center, it will be noted, if attention is focused on the peaks that occur in the 0.30, 0.35, and 0.40 ΔP_t contours (which peaks, for no spoiler and the 0.5-in. spoilers, are adjacent to the vortex centers), that the peaks move toward midspan. These peaks may be due to the proximity of the center of low static pressure of the secondary vorticity, and it is therefore suggested that the centers of gravity of the secondary vorticity move toward midspan as the inlet boundary-layer thickness increases.

Distribution of total-pressure loss. - The total-pressure-loss distribution obtained from surveys in the exit plane of the 6-inch extension and given in figure 9 can be analyzed by a plot of total-pressure loss ΔP_t as a function of the weight-flow ratio W/W_{tot} where, for each value of ΔP_t , W/W_{tot} is the percent of total weight-flow rate that has a total-pressure loss at least as high as ΔP_t . Such plots are given in figure 12 where, for example, the highest possible ΔP_t is 1.0, which occurs on the walls (at exit) where the weight-flow rate is zero. For each spoiler size, the variation in weight-flow rate W with ΔP is obtained by a numerical integration of the known areas and the known velocities between contours of constant ΔP_t in figure 9. A similar curve for the elbow inlet can be obtained for each spoiler size from the total-pressure surveys at the inlet (fig. 3), and these curves are also plotted in figure 12. If it is assumed that the same fluid particle is associated with the same value of W/W_{tot} at inlet and exit, then the increase in ΔP_t from inlet to exit is a measure of the viscous and mixing losses sustained by that particle while flowing through the elbow. (The gain in total pressure exhibited by certain fluid particles for the 2.0- and 2.5-in. spoilers, figs. 12(e) and 12(f), could result from the mixing of these particles with other particles of higher total pressure.) With the exceptions just noted, all fluid particles experience some loss in total pressure. From the standpoint of elbow efficiency (which will be given later) these losses are not excessive; however, these normal friction losses may be large as compared with the magnitude of the secondary flow losses themselves. Thus, the assumption, often made in theoretical analyses of secondary flow, that the total pressure of each fluid particle remains constant is not realistic from a quantitative viewpoint; however, the effect of this assumption on the qualitative motion of secondary flow may possibly be acceptably small.

Elbow efficiency. - If the elbow efficiency η is defined as the mass-weighted average value of the ratio of tank gage pressure minus the loss in total pressure from the inlet to the exit of the elbow, all divided by the tank gage pressure (the tank gage pressure ($P_T - P_a$) corresponds to the exit velocity head), the equation for η becomes

$$\eta = \frac{1}{W_{tot}} \int_0^{W_{tot}} \frac{(P_T - P_a) - (P_{t,i} - P_{t,e})}{P_T - P_a} dW$$

or, from equation (1),

$$\eta = 1 - \int_0^{1.0} \left[(\Delta P_t)_e - (\Delta P_t)_i \right] d\left(\frac{W}{W_{tot}}\right) \quad (2)$$

The integral in equation (2) is the area between the curves in figure 12. The resulting variation in η with spoiler size is shown in figure 13. The efficiencies for this elbow are high, as compared with those of most elbows, for all spoiler sizes, indicating that the loss in total pressure is relatively small. Although the actual loss in total pressure is small, the further losses possibly arising because of the secondary flow effects (as previously stated in the INTRODUCTION) may be important in the performance of compressors and turbines. (If, however, the elbow efficiency were based on the inlet velocity head instead of on $(P_T - P_a)$, the difference $(1 - \eta)$ would be as much as four times greater than in fig. 13.) The marked decrease in efficiency for spoiler sizes greater than 0.5 inch may be associated with the rather sudden difference in the character of the secondary flow that occurs between the 0.5- and 1.0-inch spoiler sizes, as noted previously, or may indicate that the efficiency for the 0.5-inch spoiler is out of line as a result of the somewhat different inlet velocity profile (fig. 3) for this spoiler size.

Continuity considerations. - In order to check the accuracy of the total-pressure survey data at the inlet and exit of the elbow, the weight-flow rates into and out of the elbow were computed for each spoiler size from the continuity equation

$$W = \int \rho q dA$$

where A is area (in this case, in the inlet or exit planes of the elbow) and where the velocity q is obtained from the measured total-pressure distribution (in conjunction with the assumed constant static pressure). The calculations were made for a tank gage pressure of 20 inches of water (exit Mach number of 0.26), and the dimensionless total-pressure loss contours of constant ΔP_t were assumed to be the same as those obtained for a discharge Mach number of 0.4 (fig. 9). Also, the density ρ was assumed constant over the inlet plane and the exit plane and was obtained from

$$\rho = \frac{p}{RT}$$

where R is the gas constant and where, because the velocities involved were relatively low, the tank total temperature was used for T .

The resulting integrated weight-flow rates at inlet and exit are compared for each spoiler size in the following table:

Spoiler size	W_i , lb/sec	W_e , lb/sec	Difference, percent of W_e
0	14.57	14.60	-0.21
.5	14.57	14.55	.14
1.0	14.38	14.28	.70
1.5	14.34	14.27	.49
2.0	14.21	14.29	-.56
2.5	14.11	13.98	.93

The difference in weight flows is less than 1 percent of the exit weight flow, and indicates good agreement for the total-pressure surveys. The ideal weight-flow rate for conditions of the test is 15.11 pounds per second, which indicates flow coefficients (ratios of actual to ideal flow rates) well above 0.9 in all cases.

It is interesting to note in the table that, although the inlet boundary-layer thickness increases greatly with spoiler size, the weight-flow rate through the elbow is only slightly affected. This small effect of spoiler size on weight-flow rate results because at the exit, as a result of acceleration through the elbow, a large portion of the "low"-energy flow has a relatively high velocity (although, of course, less than that of the main flow). At the elbow inlet the small effect of spoiler size on weight flow is achieved by higher velocities in the main flow as the spoiler size increases. These higher velocities result from decreasing inlet static pressure, a phenomenon which will be discussed.

Spanwise Wall-Static-Pressure Distribution

Test results. - The spanwise distribution of static pressure P on the pressure (outer) and suction (inner) surfaces of the elbow is given in table II and is shown in figure 14 for various values of φ for the same half of the elbow for which the total-pressure-loss surveys were made in figure 9. (The xy-coordinates of φ along the elbow profile are given in table I.) It might be expected that because of the lower velocities near the plane wall of the elbow less pressure difference across the channel at the same value of φ (see fig. 5) would be required there to turn the flow. Therefore, the static pressure P would fall off toward the plane wall of the elbow on the pressure surface and/or would rise toward the plane

3005
CY-2 back

wall on the suction surface. Actually, for the case of no spoiler (fig. 14(a)) there is a rapid rise (spanwise) in P on the suction surface for large values of Φ , but elsewhere on the suction surface and everywhere on the pressure surface the spanwise variation in P is negligible. As the spoiler size increases, only a small spanwise variation in P begins to appear on the pressure surface, whereas very large variations occur on the suction surface. For all spoiler sizes these large variations in P on the suction surface become most serious for values of Φ greater than 1.5. The smoke pattern in figure 15 shows that for this value of Φ the secondary flow on the plane wall has converged to the suction surface and begun to roll up. Thus, the rapid variation in spanwise distribution of P on the suction surface is associated with the formation of the passage vortex.

The distributions of static pressure P given in figure 14 have been plotted in figures 16(a) and 16(b) as a function of the velocity potential Φ for the midspan and elbow wall positions, respectively, to enable a direct comparison of the pressure distributions for the various spoiler sizes. Also included in these plots is the theoretical distribution of P for which the elbow was designed (ref. 12). This pressure is related to the prescribed (design) distribution Q , given in figure 7, by

$$P = 1 - Q^2 \quad (3)$$

For all spoiler sizes, the agreement between the prescribed and experimental distributions of P is good at the midspan position, since the influence of the secondary flows on the static pressures is not so great at midspan as near the elbow wall. Also, for all spoiler sizes, the agreement between theory and experiment is excellent on the pressure surface at the elbow wall position, but the agreement becomes progressively worse on the suction surface as the spoiler size increases because of the presence of the passage vortex.

In these plots it is of interest that near the inlet and exit of the elbow the static pressure P is slightly greater on the suction surface than on the pressure surface. The same phenomenon was observed near the exit in a theoretical analysis of two-dimensional shear flow (vorticity vector normal to the plane of flow) in the same elbow (ref. 1), and was attributed to an overturning of the average flow just upstream of the exit.

Also of interest in figure 16 is the reduction in P_1 with increasing spoiler size. This reduction in P_1 is plotted in figure 17, where the ideal value of P_1 , given by equation (3) for the design value of Q_1 (0.5), is also plotted. In reference 1, a similar decrease in P_1

was observed for increasing amounts of low-energy flow (two-dimensional shear flow) at the elbow inlet. The physical explanation is as follows: There are two opposing actions occurring in the boundary layer as it moves from the elbow inlet to the elbow exit: (1) mixing or viscous effects tend to thicken the boundary layer, and (2) acceleration effects tend to thin the boundary layer. With a thin boundary layer (that corresponding to the case for no spoiler, for example), the mixing or viscous effects predominate, causing the boundary layer to thicken somewhat as it moves through the elbow. Thus, these effects cause the main flow to occupy a smaller percentage of flow area at the exit than at the inlet. As a result, the acceleration of the main flow is increased and therefore since P_e is constant (atmospheric pressure), P_i is increased. (It may be pointed out that if the boundary-layer thickness were maintained constant throughout the elbow by changing the area ratio from inlet to exit of the elbow, the experimental value of P_i would be higher than the ideal value of P_i .) With a thick boundary layer at the inlet, the acceleration effects predominate, causing the boundary layer to thin somewhat as it moves through the elbow while the main flow experiences a smaller acceleration than it would have in the absence of the lower-energy boundary-layer flow. Thus, the main flow occupies a larger percentage of the flow area at the exit than the inlet and there is a decrease in the inlet static pressure P_i . The decrease in P_i increases with increasing inlet boundary-layer thickness (increase in spoiler size), as shown in figure 17. At some intermediate boundary-layer thickness there is a balance between these two opposing effects and the value of the inlet static pressure P_i is the same as for the ideal case. For this elbow, the experimental P_i is equal to the ideal P_i at a boundary-layer thickness corresponding to the 0.5-inch spoiler (fig. 17).

Force and momentum considerations. - In order to adopt the vortex theory of finite wings to the problem of secondary flow in elbows and other curved channels, it is necessary to focus attention not on the forces that turn the main flow (which flow is analogous to the main vortex-free flow over the airfoil) but on the excess forces that overturn the boundary-layer flow. For an isolated airfoil the maximum force on the flow occurs at the center of the wing, and as this force diminishes toward the wing tip a trailing vortex develops. For flow around an elbow the maximum excess force on the flow, over that force required to turn the prescribed amount, occurs at the wall (because here the velocities are lower and do not require the pressure gradients imposed by the main flow). As this excess force diminishes away from the wall, a passage vortex (the core of the secondary flow) develops. Thus, by analogy, the boundary layer on the elbow wall could be replaced by an imaginary, finite airfoil cantilevered from the elbow wall and extended in the

spanwise direction toward the midplane (fig. 18). This airfoil, like the boundary layer, gives rise to a trailing (passage) vortex. The airfoil is visualized as a finite lifting line located in the exit plane of the elbow, or as a lifting surface distributed around the bend of the elbow.

In figure 18 the trailing vortex has a mirror image with the plane wall of the elbow, and if it is assumed that the vortex pair trails directly downstream of the elbow, then (from ref. 13, p. 207) the impulse I of this vortex pair is given by

$$I = - \rho \Gamma b s \quad (4)$$

where Γ is the strength (circulation) of the vortex downstream of the elbow (assuming no viscosity), b is the spacing of the vortex pair, and s is the downstream length of the trailing vortices (from zero time, at which time the fluid started to flow through the elbow). The impulse I is a vector quantity that is normal to the plane of the trailing vortices and is directed toward the suction surface of the elbow. For the 90° elbow of this report the impulse is directed in the negative y -direction. Because the length s of the vortices increases with time t , the impulse I must vary with time, and its time rate of change must be equal to the force ΔF_y required to generate secondary (trailing) vorticity. Thus, from equation (4), for the 90° elbow,

$$\Delta F_y = - \frac{dI}{dt} = - \rho \Gamma b q_v \quad (5)$$

where ΔF_y is in the negative y -direction, and q_v is the velocity with which any particle of the vortex core is moving downstream. If ΔF_y , ρ , b , and q_v are determined experimentally, then equation (5) determines the strength Γ of the secondary flow.

In order to determine the magnitude of ΔF_y , consider the fluid contained in the elbow at a given instant. This fluid is enclosed in a control surface that includes the walls of the elbow and the inlet and exit planes. Ultimately the force ΔF_y must result from integrated pressure forces (acting on the control surface) in excess of the forces required to achieve the change in integrated rate of momentum flow into and out of the control surface. In terms of the y -components of these forces,

$$\Delta F_y = (F_y)_p - (F_y)_m \quad (6)$$

where the subscripts p and m refer to the pressure and momentum considerations, respectively.

The integrated pressure force acting on the control surface in the y -direction is

$$(F_y)_p = \int_{\text{surface}} p dA_y \quad (7a)$$

where A_y is the projected area of the control surface in the y -direction (positive when the outward normal is in the positive y -direction). The force required to change the integrated rate of momentum flow into and out of the control surface in the y -direction is

$$(F_y)_m = \int_{\text{surface}} \rho q_y q \cos \alpha dA \quad (7b)$$

where q_y is the y -component of q and α is the angle between the velocity vector q and the direction normal to A . For the 90° elbow of this report, equation (7b) becomes

$$(F_y)_m = - \int_{A_i} \rho q_i^2 dA_i \quad (7c)$$

which is negative because the outward normal to A_i is in the negative y -direction. Similarly, in the x -direction,

$$(F_x)_p = \int_{\text{surface}} p dA_x \quad (7d)$$

and

$$(F_x)_m = \int_{A_e} \rho q_e^2 dA_e \quad (7e)$$

where for the purpose of the integration, q_e is assumed to be in the through-flow direction.

The F_x and F_y force components have been computed from both the integrated pressure and the integrated momentum flow rates using the experimental data and equations (7a), (7c), (7d), and (7e). (The F_x values are presented here in order to give an idea of the experimental error involved in these calculations.) The results are given in figure 19 as a function of the spoiler size. (Also plotted are the theoretical

3005 values of F_x and F_y for potential flow.) From these results it is evident that the ΔF_y given by equation (6) is a relatively small quantity (and in fact has the wrong sign for the smaller spoiler sizes). Furthermore, the values of ΔF_y are not significantly different from the differences between $(F_x)_p$ and $(F_x)_m$ (which differences are experimental error), so that the magnitude of ΔF_y must be within experimental error. As ΔF_y is small and q_v is sizable (since the low-energy fluid has been accelerated as well as the main flow), it is concluded from equation (5) that the strength Γ of the secondary vorticity is small and the energy involved is small. This conclusion agrees with the findings in reference 8.

SUMMARY OF RESULTS AND CONCLUSIONS

Secondary flow tests were conducted on an accelerating elbow with 90° of turning designed for prescribed velocities that eliminate boundary-layer separation by avoiding local decelerations along the walls. Secondary flows were investigated for six boundary-layer thicknesses generated on the plane walls of the elbow by spoilers upstream of the elbow inlet. For each spoiler size, total-pressure surveys at the inlet and exit planes of the elbow and complete spanwise static-pressure distributions on the pressure and suction surfaces of the elbow were obtained. The test results were analyzed by continuity and momentum considerations in an effort to correlate the secondary flows at the exit with the inlet flow conditions and the measured wall-static-pressure distributions. Analysis of the data indicated that boundary-layer separation did not occur in the elbow and that the efficiency of this elbow was high for all spoiler sizes. The weight-flow rate of the elbow was only slightly decreased with increasing spoiler size. Results and conclusions of the tests are as follows:

1. The passage vortex associated with secondary flows in elbows might be considered to be formed by the folding up of constant total-pressure surfaces (Bernoulli surfaces) and, then, the eventual winding up of the streamlines, which lie on these surfaces, into a tight spiral. In the exit plane of the elbow, the passage vortex appears to be near the suction surface and away from the plane wall of the elbow and does not have appreciable spanwise motion as it moves downstream from the elbow exit. It is suggested that the centers of gravity of the secondary vorticity in the exit plane of the elbow move toward midspan as the inlet boundary-layer thickness on the elbow wall increases.

2. As the spoiler size increases, the boundary-layer form changes and a rather sudden difference in the secondary flow occurs, perhaps associated with the reduced importance of viscous effects in thick boundary layers.

3. If boundary-layer separation is avoided, the assumption often made in theoretical analyses of secondary flow, that the total pressure of each fluid particle remains constant, is not realistic from a quantitative viewpoint as the normal friction losses may be large compared with the secondary flow losses. However, the effect of this assumption on the qualitative motion of secondary flow may possibly be acceptably small.

4. From considerations of experimentally determined pressure forces exerted by the elbow on the flow and of momentum flow rates through the elbow, it is suggested that the strength of the secondary vortices is small and the energy of the secondary flows is small.

5. For all spoiler sizes the agreement between prescribed and experimental static pressures was good on the entire pressure surface and at the midspan position of the suction surface; however, a discrepancy existed along the suction surface near the elbow plane wall for values of velocity potential greater than 1.5, which may be associated with the formation of the passage vortex as shown by smoke studies.

Lewis Flight Propulsion Laboratory
National Advisory Committee for Aeronautics
Cleveland, Ohio, July 22, 1953

APPENDIX - SYMBOLS

The following symbols are used in this report:

A	area
b	spacing of secondary vortex pair, fig. 18
F	force acting on fluid in elbow
I	impulse of secondary vortex pair, fig. 18
P	dimensionless pressure, eq. (1)
p	pressure
Q	velocity ratio, local velocity expressed as ratio of downstream exit velocity
q	velocity
R	gas constant
s	downstream length of secondary vortex
T	temperature
t	time
W	weight-flow rate
w	elbow span, fig. 1
x,y,z	Cartesian coordinates, fig. 1
α	angle between velocity vector q and direction normal to surface area
Γ	strength of secondary vortex
ΔF_y	difference between y-component of pressure force exerted on fluid in elbow and force required by changes in y-component of momentum flow rate through elbow
ΔP_t	loss in dimensionless total pressure
η	elbow efficiency, eq. (2)
ρ	weight density
ϕ	velocity potential, dummy variable along curved walls of elbow

3005

CY-3

Subscripts:

a atmospheric
e elbow exit
i elbow inlet
m from momentum considerations
max maximum
p from pressure considerations
T tank
t total
tot total (summation)
v vortex
x,y x- and y-components, respectively

REFERENCES

1. Kramer, James J., and Stanitz, John D.: Two-Dimensional Shear Flow in a 90° Elbow. NACA TN 2736, 1952.
2. Wirt, Loring: New Data for the Design of Elbows in Duct Systems. Gen. Elec. Rev., vol. 30, no. 6, June 1927, pp. 286-296.
3. Weske, John R.: Experimental Investigation of Velocity Distributions Downstream of Single Duct Bends. NACA TN 1471, 1948.
4. Allen, Hubert W., Kofskey, Milton G., and Chammess, Richard E.: Experimental Investigation of Loss in an Annular Cascade of Turbine Nozzle Blades of Free Vortex Design. NACA TN 2871, 1953.
5. Rohlik, Harold E., Allen, Hubert W., and Herzig, Howard Z.: Study of Secondary-Flow Patterns in an Annular Cascade of Turbine Nozzle Blades with Vortex Design. NACA TN 2909, 1953.
6. Kofskey, Milton G., Allen, Hubert W., and Herzig, Howard Z.: Comparison of Secondary Flows and Boundary-Layer Accumulations in Several Turbine Nozzles. NACA TN 2989, 1953.

7. Hansen, Arthur G., Herzig, Howard Z., and Costello, George R.: A Visualization Study of Secondary Flows in Cascades. NACA TN 2947, 1953.
8. Eichenberger, Hans P.: Shear Flow in Bends. Tech. Report No. 2, Office Naval Res., Gas Turbine Lab., M.I.T., Apr. 15, 1952. (Contract N5ori07848.)
9. Squire, H. B., and Winter, K. G.: The Secondary Flow in a Cascade of Airfoils in a Nonuniform Stream. Jour. Aero. Sci., vol. 18, no. 4, Apr. 1951, pp. 271-277.
10. Hawthorne, William R.: Secondary Circulation in Fluid Flow. Proc. Roy. Soc. (London), ser. A, vol. 206, no. A1086, May 7, 1951, pp. 374-387.
11. Kronauer, Richard E.: Secondary Flow in Fluid Dynamics. Doctoral Thesis, Harvard Univ., Mar. 7, 1951. (See also Pratt and Whitney Res. Rep. No. 132, Gordon McKay Lab., Harvard Univ., Apr. 1951.)
12. Stanitz, John D.: Design of Two-Dimensional Channels with Prescribed Velocity Distributions Along the Channel Walls. I - Relaxation Solutions. NACA TN 2593, 1952.
13. Milne-Thomson, L. M.: Theoretical Aerodynamics. D. Van Nostrand Co., Inc., 1947.

3005


CY-3 back

TABLE I. - COORDINATES AND PRESCRIBED VELOCITY Q ALONG
CURVED WALLS OF ELBOW (REF. 12)



ϕ^1	Suction (inner) surface			Pressure (outer) surface		
	Q	x , in.	y , in.	Q	x , in.	y , in.
-0.750	0.5000	5.95	-8.82	0.5000	-5.97	-8.82
-.625	.5000	5.94	-7.33	.5000	-5.97	-7.33
-.500	.5000	5.93	-5.84	.5000	-5.96	-5.84
-.375	.5000	5.91	-4.34	.5000	-5.94	-4.34
-.250	.5000	5.90	-2.86	.5000	-5.93	-2.85
-.125	.5000	5.86	-1.36	.5000	-5.90	-1.36
0	.5000	5.81	0.13	.5000	-5.86	0.14
.125	.5097	5.70	1.61	.5000	-5.80	1.63
.250	.5354	5.56	3.05	.5000	-5.72	3.12
.375	.5715	5.38	4.38	.5000	-5.62	4.61
.500	.6134	5.23	5.63	.5000	-5.48	6.10
.625	.6576	5.11	6.80	.5000	-5.29	7.58
.750	.7018	5.04	7.90	.5000	-5.07	9.06
.875	.7448	5.02	8.93	.5000	-4.77	10.52
<u>1.000</u>	.7855	5.07	9.90	.5000	-4.41	11.96
1.125	.8235	5.17	10.82	.5000	-3.97	13.39
1.250	.8583	5.33	11.70	.5000	-3.45	14.80
1.375	.8898	5.56	12.52	.5000	-2.85	16.16
1.500	.9177	5.85	13.30	.5000	-2.16	17.48
<u>1.625</u>	.9418	6.19	14.02	.5000	-1.37	18.75
1.750	.9620	6.58	14.70	.5000	-0.49	19.96
1.875	.9782	7.03	15.33	.5000	.48	21.09
<u>2.000</u>	.9901	7.53	15.90	.5000	1.55	22.14
<u>2.125</u>	.9975	8.06	16.42	.5000	2.69	23.09
2.250	1.0000	8.64	16.89	.5000	3.93	23.92
2.375	1.0000	9.26	17.32	.5097	5.26	24.60

¹Underlined values of ϕ indicate location of spanwise static-pressure taps.

TABLE I. - COORDINATES AND PRESCRIBED VELOCITY Q ALONG
CURVED WALLS OF ELBOW (REF. 12) - Concluded 

ϕ^1	Suction (inner) surface			Pressure (outer) surface		
	Q	x , in.	y , in.	Q	x , in.	y , in.
<u>2.500</u>	1.0000	9.91	17.69	0.5354	6.60	25.11
<u>2.625</u>	1.0000	10.58	18.02	.5715	7.91	25.44
2.750	1.0000	11.27	18.30	.6134	9.15	25.65
2.875	1.0000	11.98	18.55	.6576	10.32	25.77
<u>3.000</u>	1.0000	12.69	18.75	.7018	11.41	25.83
<u>3.125</u>	1.0000	13.42	18.92	.7448	12.45	25.85
3.250	1.0000	14.15	19.06	.7855	13.42	25.84
3.375	1.0000	14.89	19.18	.8235	14.35	25.82
<u>3.500</u>	1.0000	15.63	19.28	.8583	15.24	25.79
<u>3.625</u>	1.0000	16.37	19.35	.8898	16.09	25.75
3.750	1.0000	17.11	19.41	.9177	16.92	25.71
3.875	1.0000	17.86	19.45	.9418	17.72	25.68
<u>4.000</u>	1.0000	18.61	19.50	.9620	18.50	25.65
<u>4.125</u>	1.0000	19.35	19.53	.9782	19.27	25.62
4.250	1.0000	20.10	19.55	.9901	20.03	25.61
4.375	1.0000	20.85	19.57	.9975	20.77	25.60
<u>4.500</u>	1.0000	21.59	19.59	1.0000	21.52	25.59
<u>4.625</u>	1.0000	22.34	19.60	1.0000	22.27	25.59
4.750	1.0000	23.09	19.61	1.0000	23.01	25.60
4.875	1.0000	23.83	19.62	1.0000	23.76	25.61
5.000	1.0000	24.58	19.63	1.0000	24.51	25.61

¹Underlined values of ϕ indicate location of spanwise static-pressure taps.

TABLE II. - VALUES OF SPANWISE STATIC-PRESSURE RATIO

Spoiler size, in.	Velocity potential, ϕ	Pressure surface										
		z/w										
		0.0076	0.0227	0.0379	0.0682	0.0985	0.1591	0.2197	0.2803	0.3485	0.4242	0.5000
Spanwise static-pressure ratio, P												
0	-0.5000	0.7637	0.7616	0.7631	0.7637	0.7616	0.7631	0.7626	0.7631	0.7626	0.7626	0.7591
	.0000	.7581	.7576	.7596	.7608	.7616	.7611	.7611	.7611	.7601	.7591	.7591
	.5000	.7536	.7556	.7561	.7586	.7586	.7601	.7586	.7596	.7586	.7546	.7551
	1.0000	.7481	.7496	.7516	.7536	.7526	.7551	.7531	.7546	.7541	.7521	.7506
	1.5000	.7481	.7511	.7511	.7526	.7521	.7521	.7521	.7531	.7526	.7496	.7491
	2.0000	.7561	.7571	.7576	.7566	.7576	.7586	.7571	.7566	.7541	.7521	.7536
	2.5000	.7231	.7246	.7236	.7231	.7231	.7231	.7216	.7226	.7191	.7186	.7206
	3.0000	.5443	.5453	.5483	.5438	.5418	.5395	.5348	.5343	.5308	.5263	.5268
0.5	-0.5000	0.7525	0.7500	0.7520	0.7530	0.7500	0.7535	0.7540	0.7540	0.7530	0.7530	0.7480
	.0000	.7450	.7450	.7460	.7470	.7490	.7490	.7500	.7500	.7500	.7490	.7505
	.5000	.7410	.7435	.7435	.7450	.7460	.7500	.7500	.7510	.7515	.7465	.7475
	1.0000	.7360	.7360	.7370	.7385	.7405	.7450	.7460	.7475	.7475	.7455	.7415
	1.5000	.7330	.7360	.7340	.7360	.7365	.7410	.7420	.7455	.7455	.7445	.7445
	2.0000	.7415	.7410	.7410	.7410	.7450	.7490	.7505	.7510	.7495	.7495	.7505
	2.5000	.7115	.7140	.7115	.7115	.7105	.7175	.7190	.7200	.7200	.7200	.7220
	3.0000	.5390	.5390	.5395	.5340	.5340	.5355	.5365	.5375	.5335	.5290	.5280
1.0	-0.5000	0.7275	0.7250	0.7265	0.7275	0.7265	0.7285	0.7285	0.7285	0.7300	0.7280	0.7260
	.0000	.7235	.7235	.7250	.7260	.7260	.7280	.7310	.7310	.7310	.7310	.7315
	.5000	.7190	.7200	.7200	.7230	.7240	.7290	.7300	.7315	.7340	.7310	.7320
	1.0000	.7160	.7160	.7160	.7170	.7200	.7260	.7270	.7320	.7350	.7310	.7310
	1.5000	.7160	.7160	.7175	.7175	.7190	.7225	.7260	.7325	.7325	.7335	.7350
	2.0000	.7270	.7270	.7270	.7270	.7310	.7360	.7400	.7410	.7440	.7440	.7435
	2.5000	.7000	.7025	.7015	.6985	.6965	.7000	.7035	.7115	.7150	.7180	.7190
	3.0000	.5280	.5280	.5290	.5200	.5180	.5230	.5290	.5330	.5315	.5330	.5330
1.5	-0.5000	0.6969	0.6949	0.6959	0.6969	0.6969	0.6994	0.7004	0.7024	0.7029	0.7034	0.7004
	.0000	.6984	.6974	.6969	.6979	.7014	.7019	.7054	.7054	.7084	.7089	.7089
	.5000	.6959	.6954	.6964	.6984	.6999	.7054	.7079	.7114	.7134	.7104	.7124
	1.0000	.6929	.6929	.6929	.6949	.6964	.7044	.7069	.7134	.7164	.7149	.7134
	1.5000	.6984	.6994	.6984	.6999	.6994	.7054	.7109	.7174	.7199	.7184	.7209
	2.0000	.7164	.7154	.7154	.7144	.7144	.7189	.7234	.7290	.7290	.7290	.7340
	2.5000	.6944	.6954	.6939	.6909	.6884	.6934	.6979	.7039	.7064	.7079	.7124
	3.0000	.5240	.5251	.5251	.5170	.5125	.5125	.5175	.5245	.5276	.5296	.5316
2.0	-0.5000	0.6727	0.6707	0.6722	0.6722	0.6722	0.6732	0.6772	0.6782	0.6787	0.6797	0.6757
	.0000	.6712	.6712	.6717	.6727	.6742	.6752	.6802	.6807	.6847	.6852	.6857
	.5000	.6727	.6717	.6737	.6742	.6752	.6797	.6847	.6897	.6937	.6937	.6917
	1.0000	.6717	.6727	.6742	.6757	.6767	.6817	.6872	.6957	.7007	.7002	.6982
	1.5000	.6837	.6847	.6827	.6812	.6807	.6857	.6952	.7017	.7082	.7087	.7097
	2.0000	.7072	.7087	.7082	.7047	.7037	.7047	.7121	.7156	.7216	.7231	.7281
	2.5000	.6892	.6917	.6892	.6852	.6797	.6832	.6887	.6982	.7037	.7092	.7101
	3.0000	.5232	.5217	.5237	.5137	.5088	.5045	.5117	.5242	.5297	.5317	.5317
2.5	-0.5000	0.6484	0.6469	0.6474	0.6479	0.6469	0.6489	0.6513	0.6528	0.6538	0.6558	0.6523
	.0000	.6479	.6479	.6479	.6489	.6489	.6503	.6538	.6573	.6593	.6613	.6628
	.5000	.6479	.6484	.6484	.6494	.6513	.6553	.6608	.6668	.6693	.6708	.6733
	1.0000	.6498	.6498	.6508	.6508	.6518	.6603	.6668	.6763	.6813	.6818	.6808
	1.5000	.6648	.6648	.6648	.6633	.6633	.6663	.6753	.6843	.6908	.6943	.6973
	2.0000	.6958	.6958	.6958	.6913	.6893	.6908	.6958	.7038	.7088	.7148	.7213
	2.5000	.6788	.6798	.6798	.6738	.6693	.6693	.6748	.6858	.6973	.7073	.7123
	3.0000	.5125	.5115	.5130	.5025	.4965	.4900	.4970	.5125	.5280	.5360	.5375

P FOR SIX SPOILER SIZES (FIG. 14)

Suction surface									
z/w									
0.0076	0.0227	0.0379	0.0682	0.0985	0.1591	0.2197	0.2803	0.3485	0.4242
Spanwise static-pressure ratio, P									
0.7601	0.7626	0.7611	0.7616	0.7616	0.7626	0.7616	0.7616	0.7611	0.7626
.7626	.7636	.6701	.7606	.7596	.7606	.7596	.7631	.7616	.7631
.6552	.6532	.6567	.6537	.6537	.6527	.6502	.6497	.6497	.6432
.4443	.4353	.4433	.4298	.4348	.4338	.4348	.4348	.4318	.4298
.2564	.2484	.2424	.2349	.2299	.2224	.2169	.2244	.2109	.2124
.1599	.1289	.1314	.1219	.1139	.0915	.0870	.0910	.0825	.0715
.1939	.1055	.0780	.0855	.0980	.0845	.0805	.0760	.0665	.0715
.1699	.0995	.0500	.0405	.0585	.0615	.0565	.0510	.0400	.0435
.1294	.0895	.0365	.0125	.0075	.0475	.0440	.0380	.0335	.0295
.1000	.0830	.0400	.0145	.0035	.0295	.0330	.0305	.0190	.0180
.0605	.0650	.0245	.0140	.0050	.0040	.0270	.0200	.0145	.0130
0.7475	0.7475	0.7465	0.7465	0.7465	0.7480	0.7470	0.7470	0.7470	0.7480
.7480	.7490	.7440	.7440	.7440	.7470	.7470	.7505	.7495	.7510
.6480	.6450	.6435	.6415	.6410	.6385	.6345	.6360	.6355	.6330
.4425	.4335	.4415	.4265	.4290	.4250	.4220	.4200	.4160	.4145
.2655	.2555	.2505	.2420	.2345	.2195	.2080	.2120	.1970	.1960
.1830	.1500	.1445	.1345	.1235	.0950	.0840	.0830	.0720	.0595
.2220	.1370	.0985	.0865	.1005	.0880	.0800	.0710	.0570	.0620
.1950	.1400	.0785	.0525	.0460	.0625	.0595	.0510	.0375	.0395
.1460	.1260	.0655	.0170	.0115	.0315	.0470	.0410	.0335	.0290
.1115	.1115	.0700	.0190	.0035	-.0030	.0300	.0335	.0215	.0185
.0700	.0860	.0520	.0210	.0035	-.0075	.0160	.0220	.0195	.0155
0.7301	0.7301	0.7246	0.7256	0.7246	0.7256	0.7246	0.7246	0.7246	0.7271
.7286	.7286	.7246	.7271	.7271	.7296	.7296	.7346	.7346	.7346
.6360	.6350	.6340	.6315	.6265	.6265	.6215	.6205	.6190	.6155
.4482	.4412	.4482	.4318	.4318	.4203	.4143	.4089	.3994	.3959
.2859	.2789	.2699	.2590	.2475	.2226	.2052	.2027	.1853	.1803
.2077	.1778	.1693	.1569	.1419	.1061	.0901	.0822	.0672	.0513
.2366	.1668	.1285	.1046	.1126	.0946	.0876	.0787	.0613	.0538
.2042	.1673	.1096	.0712	.0573	.0583	.0623	.0548	.0448	.0423
.1519	.1419	.0921	.0374	.0224	.0224	.0398	.0448	.0423	.0374
.1155	.1195	.0872	.0339	.0149	-.0025	.0100	.0274	.0274	.0299
.0747	.0921	.0667	.0349	.0085	-.0040	.0000	.0110	.0209	.0234
0.7046	0.7036	0.7001	0.7011	0.6996	0.7001	0.7001	0.7001	0.7001	0.7006
.7061	.7061	.7041	.7056	.7056	.7085	.7090	.7150	.7140	.7150
.6261	.6236	.6251	.6202	.6187	.6142	.6063	.6053	.6028	.6033
.4543	.4479	.4518	.4364	.4330	.4181	.4057	.3942	.3833	.3764
.3133	.3014	.2959	.2825	.2686	.2344	.2085	.1976	.1703	.1643
.2582	.2214	.2090	.1892	.1693	.1246	.0983	.0849	.0641	.0432
.2860	.2249	.1723	.1291	.1296	.1053	.0899	.0789	.0636	.0606
.2388	.2190	.1614	.0958	.0660	.0531	.0601	.0581	.0536	.0516
.1743	.1797	.1385	.0641	.0293	.0119	.0204	.0402	.0516	.0541
.1360	.1504	.1261	.0606	.0194	-.0159	-.0104	.0139	.0308	.0427
.0943	.1142	.1023	.0596	.0189	-.0179	-.0179	-.0099	.0164	.0348
0.6758	0.6758	0.6733	0.6753	0.6758	0.6768	0.6753	0.6763	0.6763	0.6778
.6818	.6808	.6728	.6763	.6773	.6838	.6833	.6909	.6904	.6914
.6088	.6048	.6058	.6043	.6018	.5953	.5863	.5843	.5788	.5783
.4507	.4442	.4472	.4347	.4287	.4097	.3912	.3762	.3607	.3537
.3112	.3037	.2962	.2846	.2686	.2331	.1996	.1831	.1516	.1426
.2516	.2206	.2091	.1901	.1711	.1251	.0951	.0770	.0540	.0295
.2631	.2131	.1711	.1336	.1346	.1086	.0901	.0745	.0625	.0740
.2191	.1976	.1491	.1011	.0735	.0600	.0565	.0515	.0505	.0555
.1651	.1611	.1256	.0655	.0365	.0165	.0200	.0315	.0440	.0565
.1261	.1316	.1126	.0600	.0250	-.0050	-.0050	.0100	.0250	.0460
.0890	.1056	.0911	.0585	.0245	-.0060	-.0135	-.0110	.0090	.0340
0.6485	0.6485	0.6480	0.6495	0.6495	0.6500	0.6500	0.6505	0.6520	0.6540
.6545	.6545	.6465	.6470	.6510	.6550	.6585	.6655	.6665	.6690
.5870	.5860	.5870	.5835	.5820	.5740	.5650	.5620	.5575	.5515
.4440	.4390	.4420	.4280	.4230	.3985	.3775	.3570	.3385	.3285
.3335	.3235	.3125	.2950	.2775	.2330	.1925	.1685	.1330	.1200
.3080	.2650	.2430	.2150	.1910	.1350	.0960	.0720	.0475	.0200
.3165	.2915	.2260	.1455	.1325	.1095	.0885	.0705	.0620	.0605
.2550	.2650	.2190	.1315	.0700	.0375	.0460	.0490	.0540	.0685
.1900	.2065	.1810	.0985	.0425	-.0105	-.0105	.0150	.0460	.0695
.1490	.1650	.1610	.0910	.0395	-.0255	-.0350	-.0165	.0165	.0545
.1065	.1260	.1275	.0885	.0370	-.0235	-.0375	-.0375	-.0105	.0375

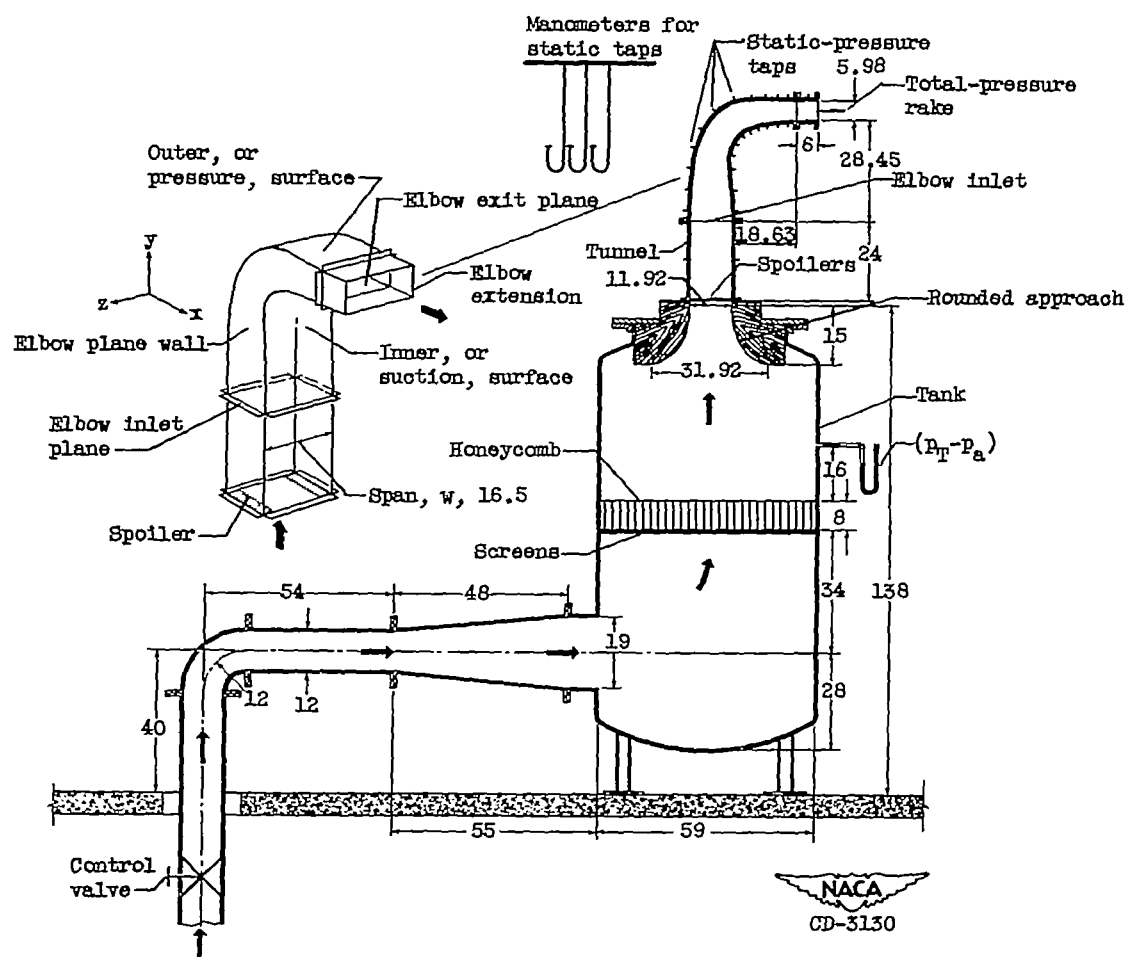


Figure 1. - Line drawing of test setup. All linear dimensions in inches.

CY-4

3005

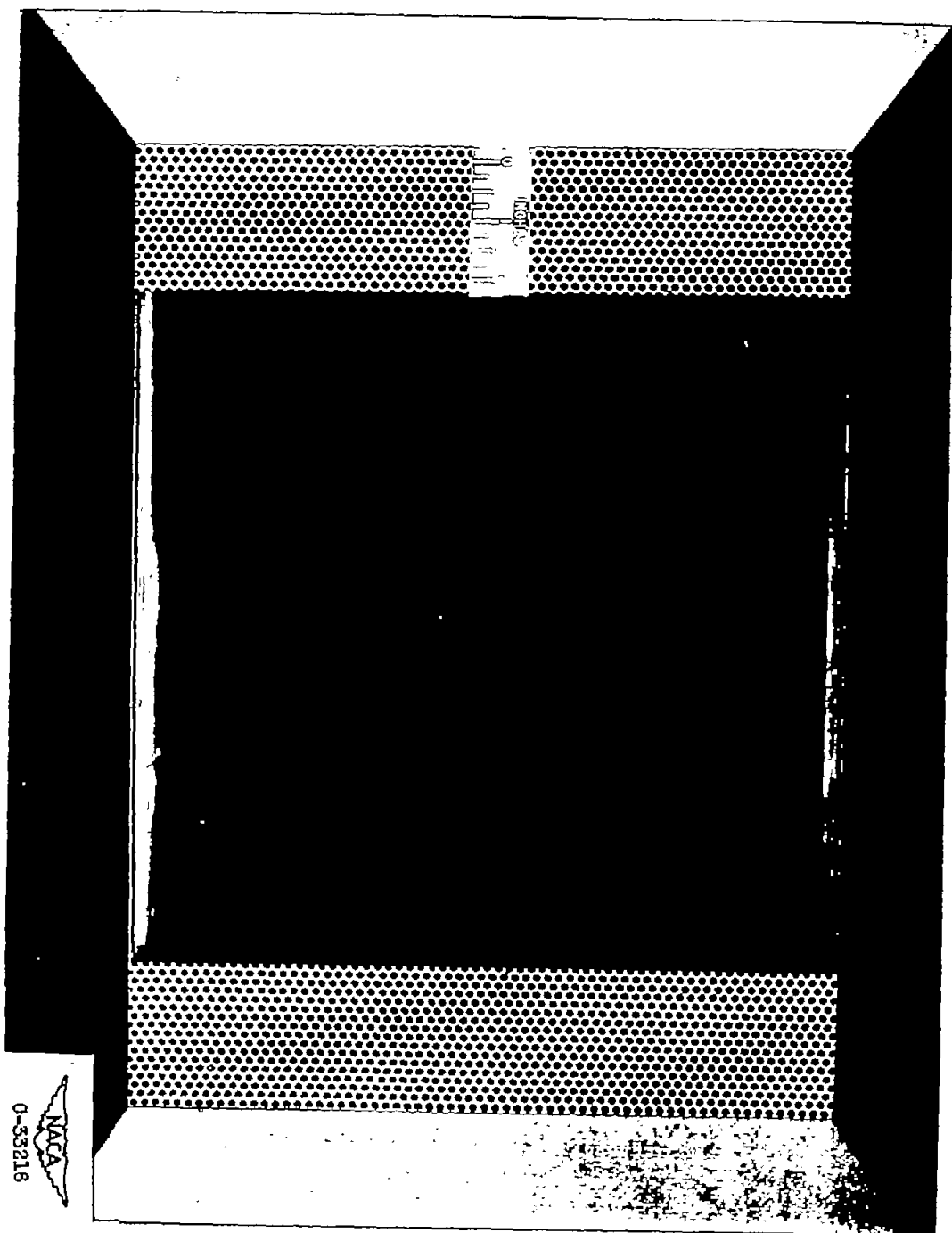


Figure 2. - Photograph of spoilers installed in tunnel. Downstream view.

NACA
0-35216

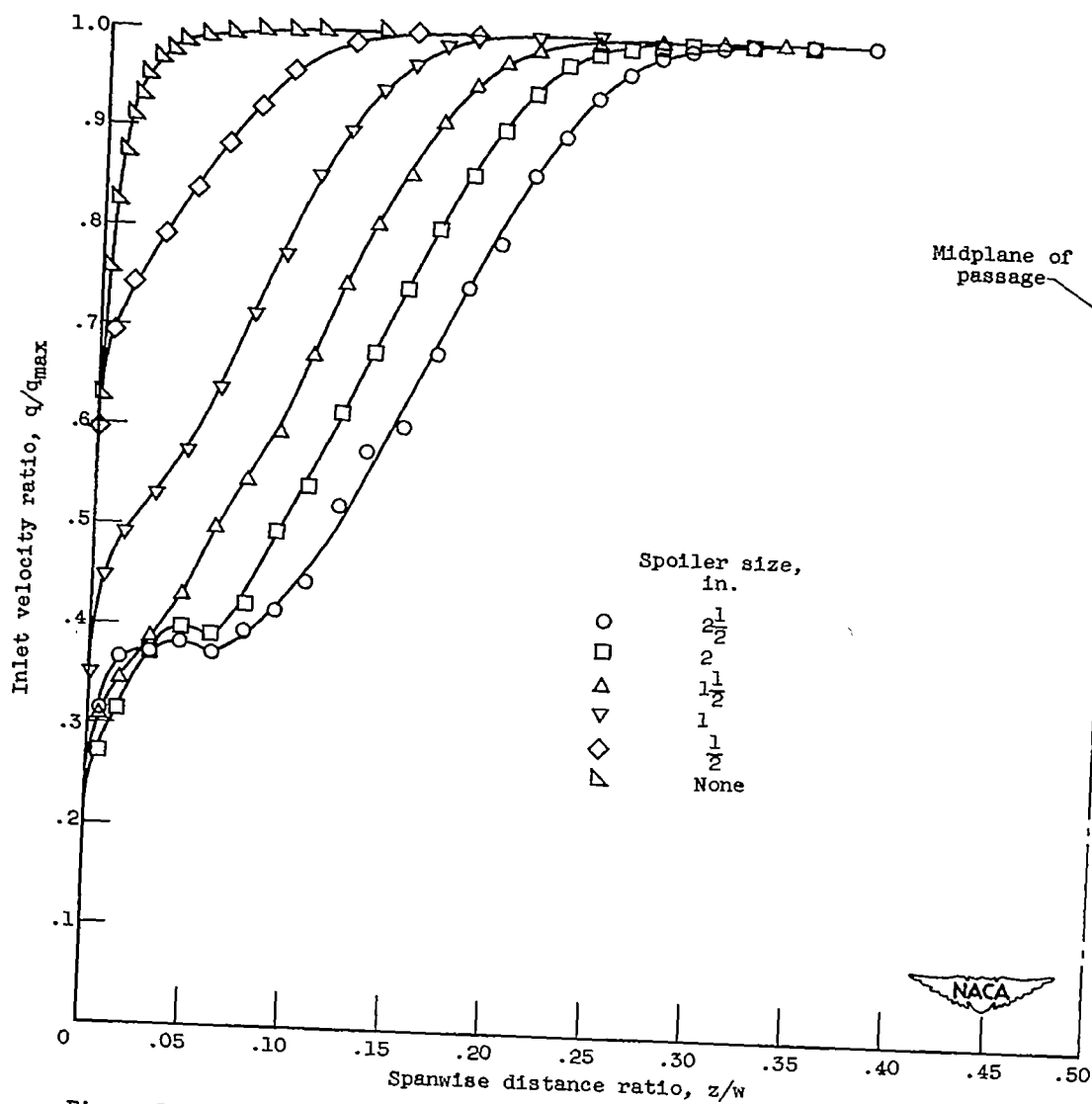
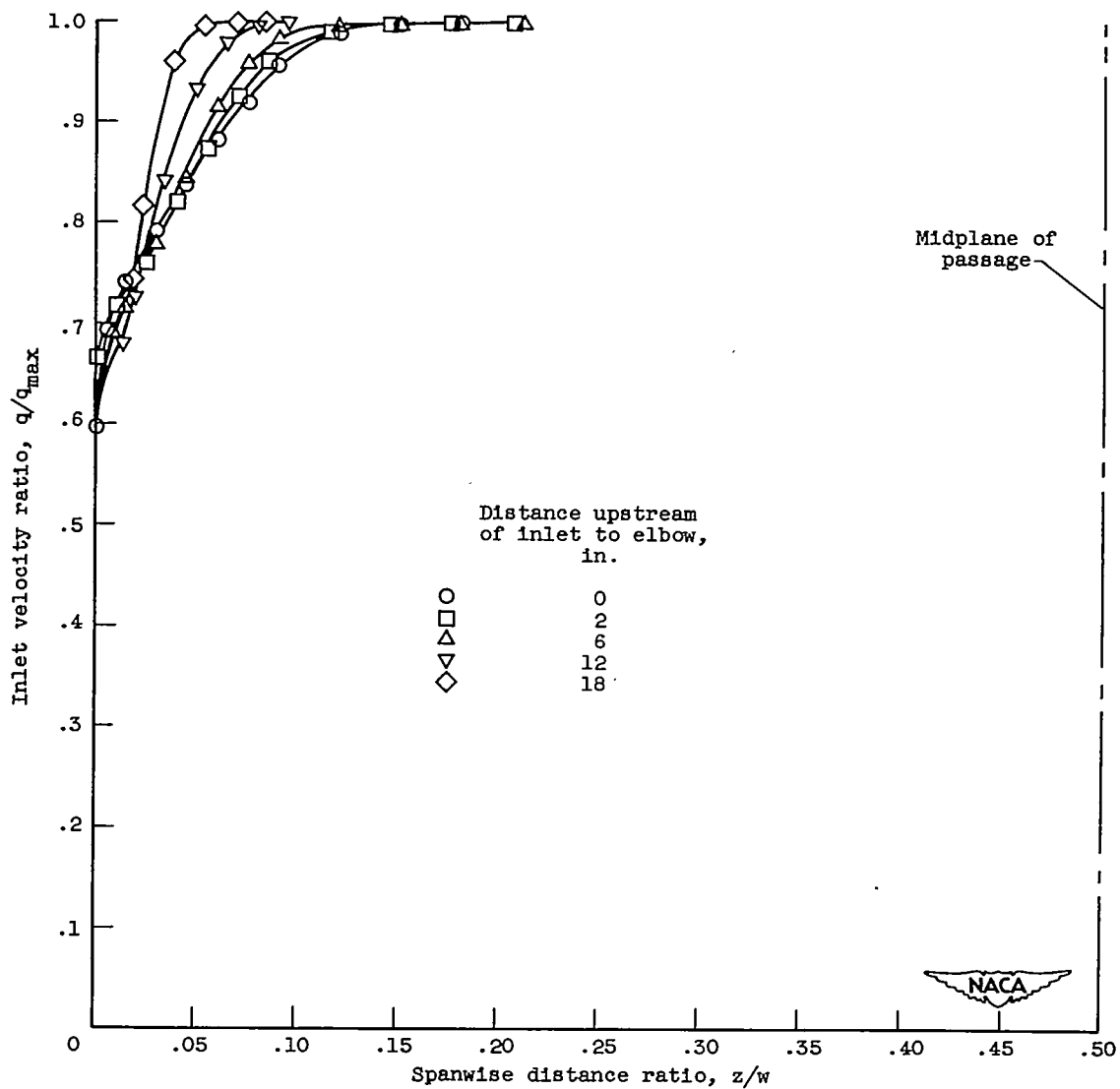


Figure 3. - Inlet velocity profiles on plane walls of elbow at center line for various spoiler sizes. Tank gage pressure ($P_T - P_a$), 20 inches of water.



(a) 0.5-Inch spoiler.

Figure 4. - Velocity profiles on plane walls of tunnel at center line for various distances upstream of inlet to elbow. Tank gage pressure ($p_T - p_a$), 20 inches of water.

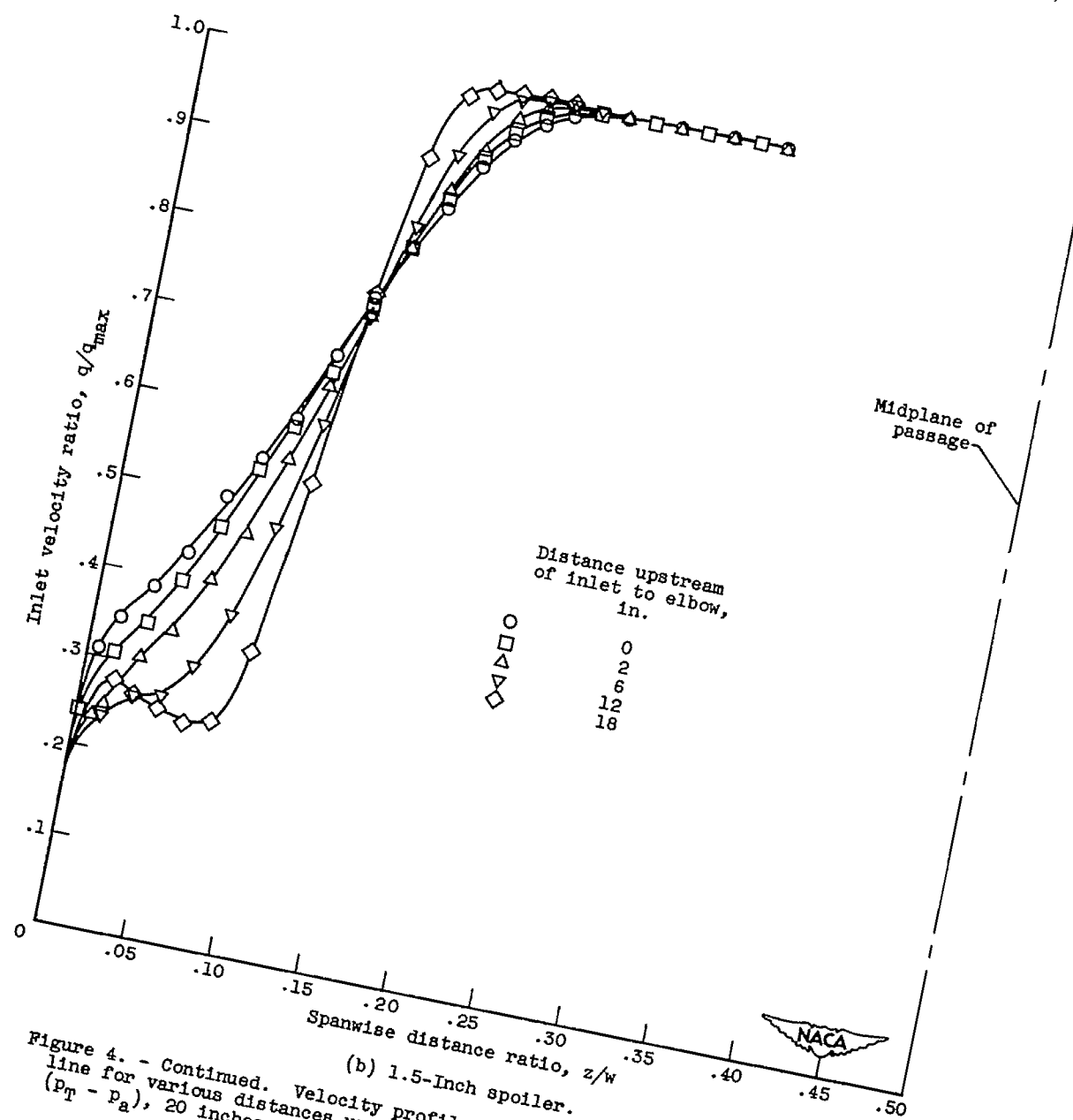


Figure 4. - Continued. Velocity profiles on plane walls of tunnel at center line for various distances upstream of inlet to elbow. Tank gage pressure ($p_T - p_a$), 20 inches of water.

(b) 1.5-Inch spoiler.

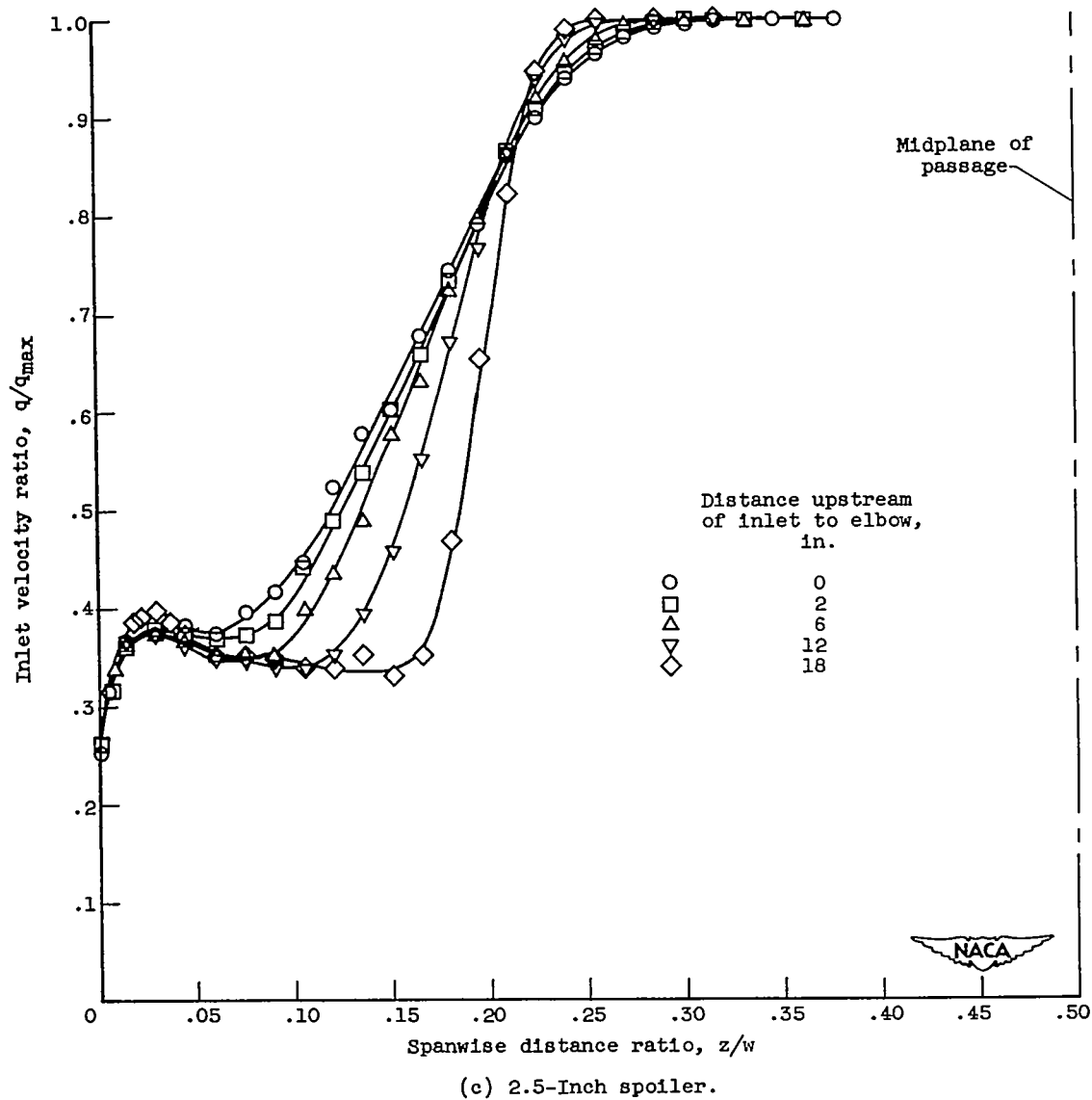


Figure 4. - Concluded. Velocity profiles on plane walls of tunnel at center line for various distances upstream of inlet to elbow. Tank gage pressure ($p_T - p_a$), 20 inches of water.

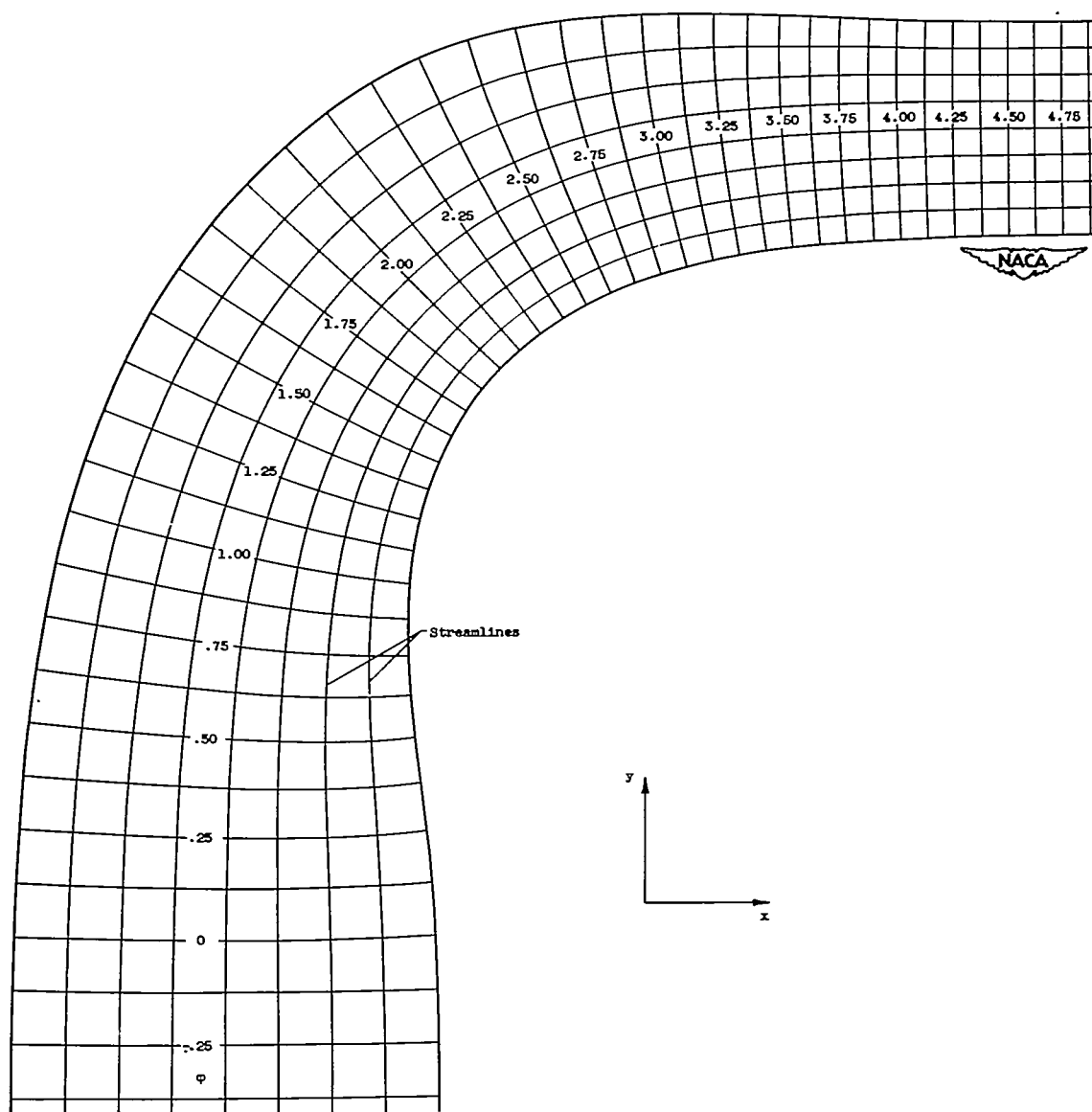


Figure 5. - Streamlines and velocity-potential lines in elbow plane. Incompressible flow; prescribed velocity given in table I.

3005

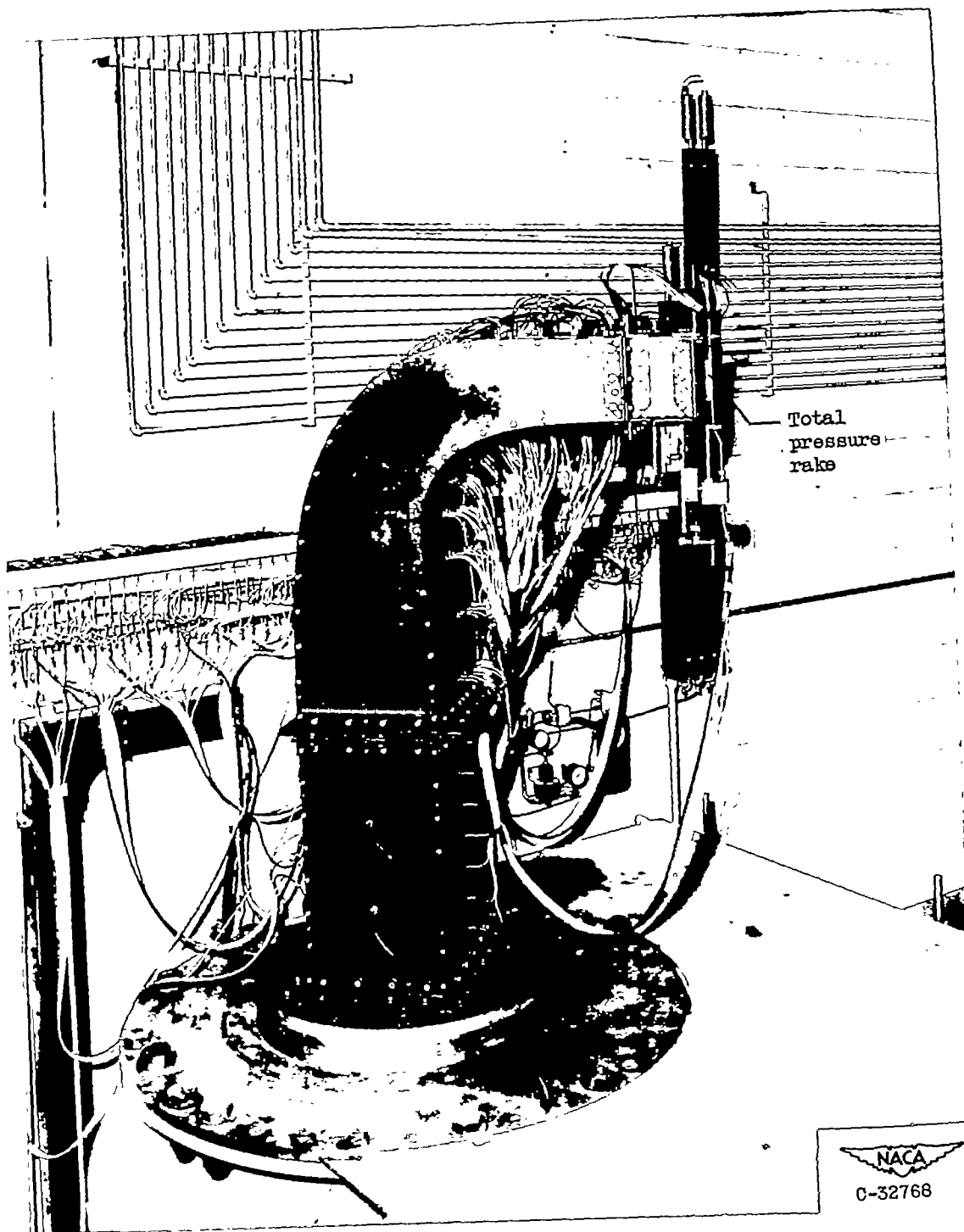


Figure 6. - Photograph of elbow installed on tank.

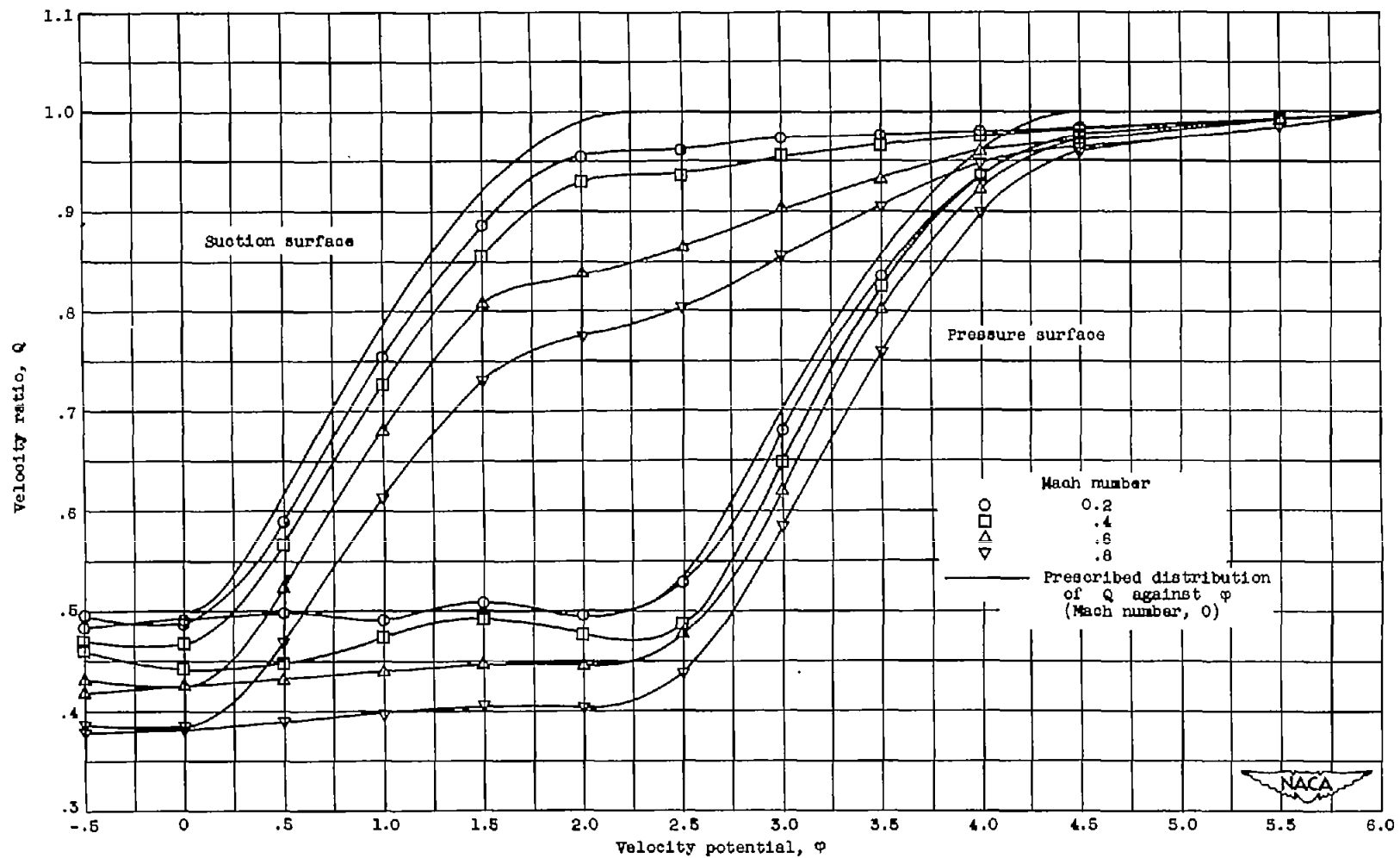
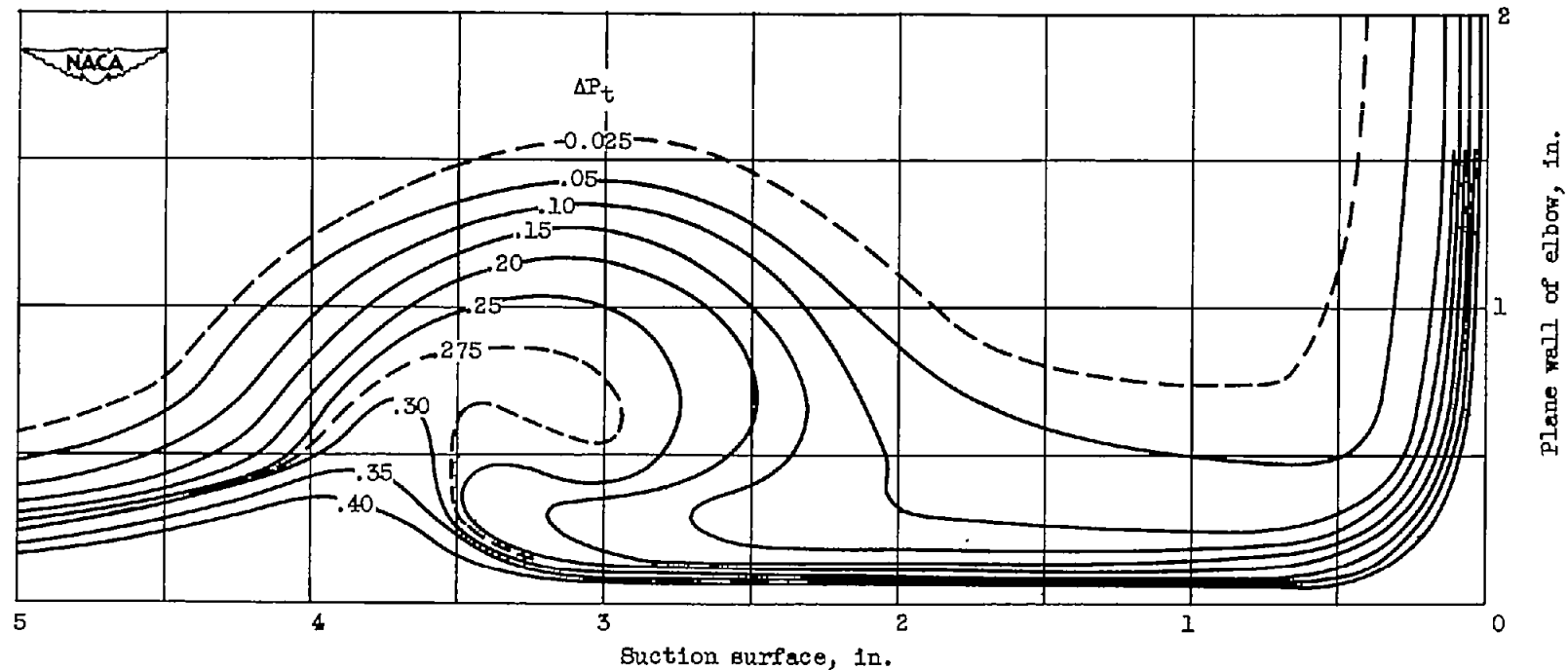
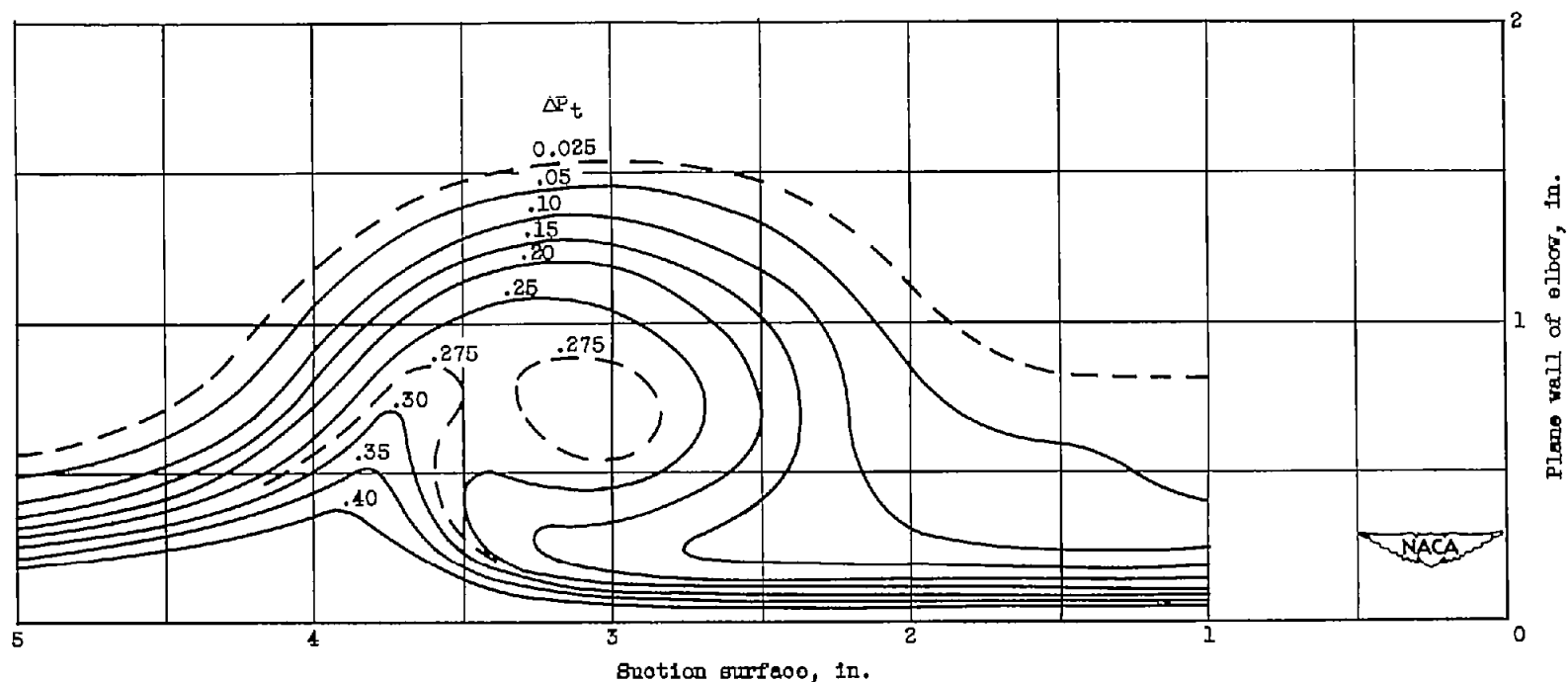


Figure 7. - Variation in velocity ratio Q with velocity potential ϕ along curved walls of elbow for various values of exit Mach number at midspan.



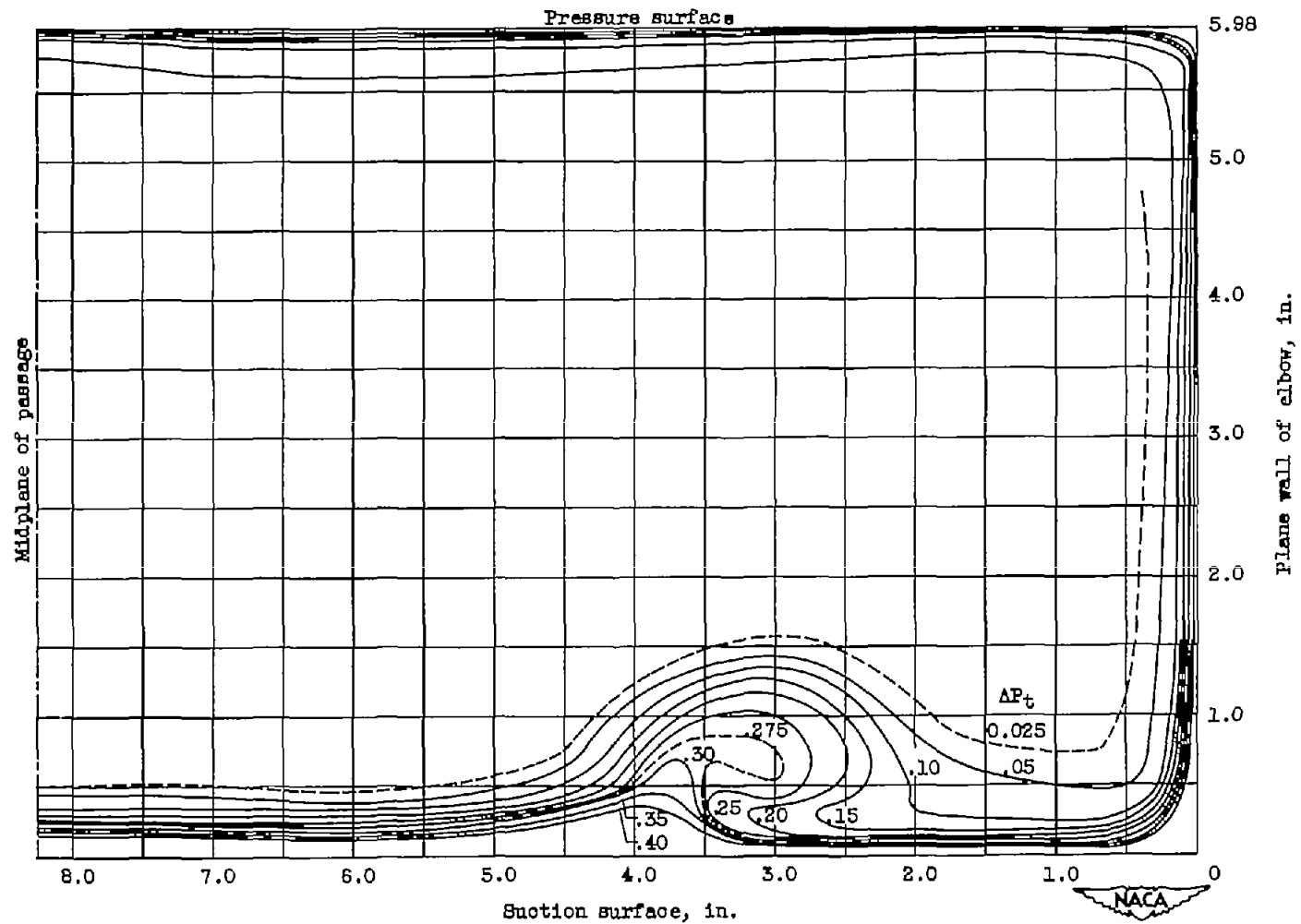
(a) Unshielded total-pressure probe.

Figure 8. - Total-pressure-loss contours of constant ΔP_t in region of secondary flow at exit plane from 6-inch extension downstream of elbow with no spoiler; shielded and unshielded total-pressure probes. Exit Mach number, 0.4 (tank gage pressure ($p_T - p_a$), 46 in. water).



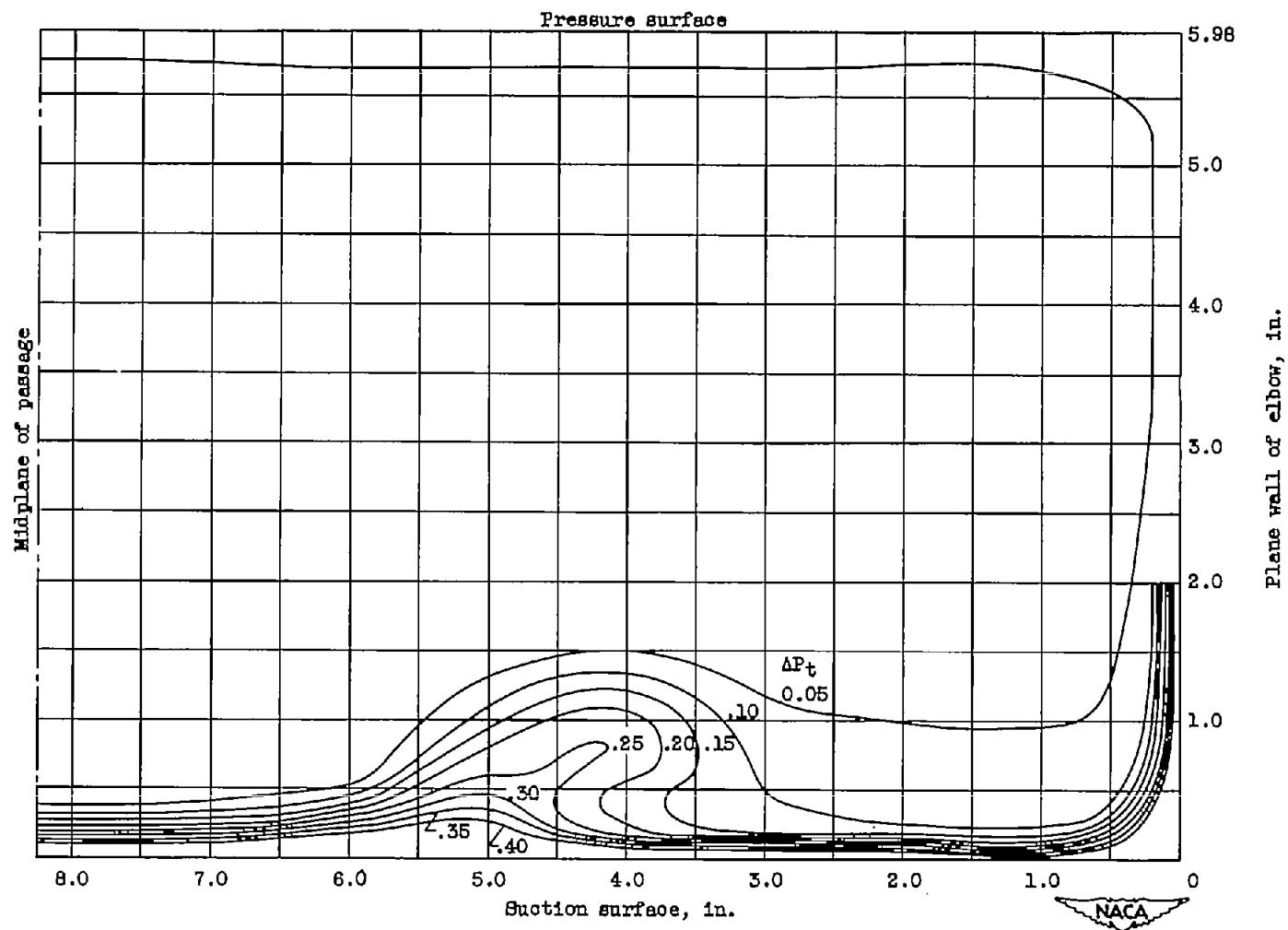
(b) Shielded total-pressure probe.

Figure 8. - Concluded. Total-pressure-loss contours of constant ΔP_t in region of secondary flow at exit plane from 6-inch extension downstream of elbow with no spoiler; shielded and unshielded total-pressure probes. Exit Mach number, 0.4 (tank gage pressure ($p_T - p_a$), 46 in. water).



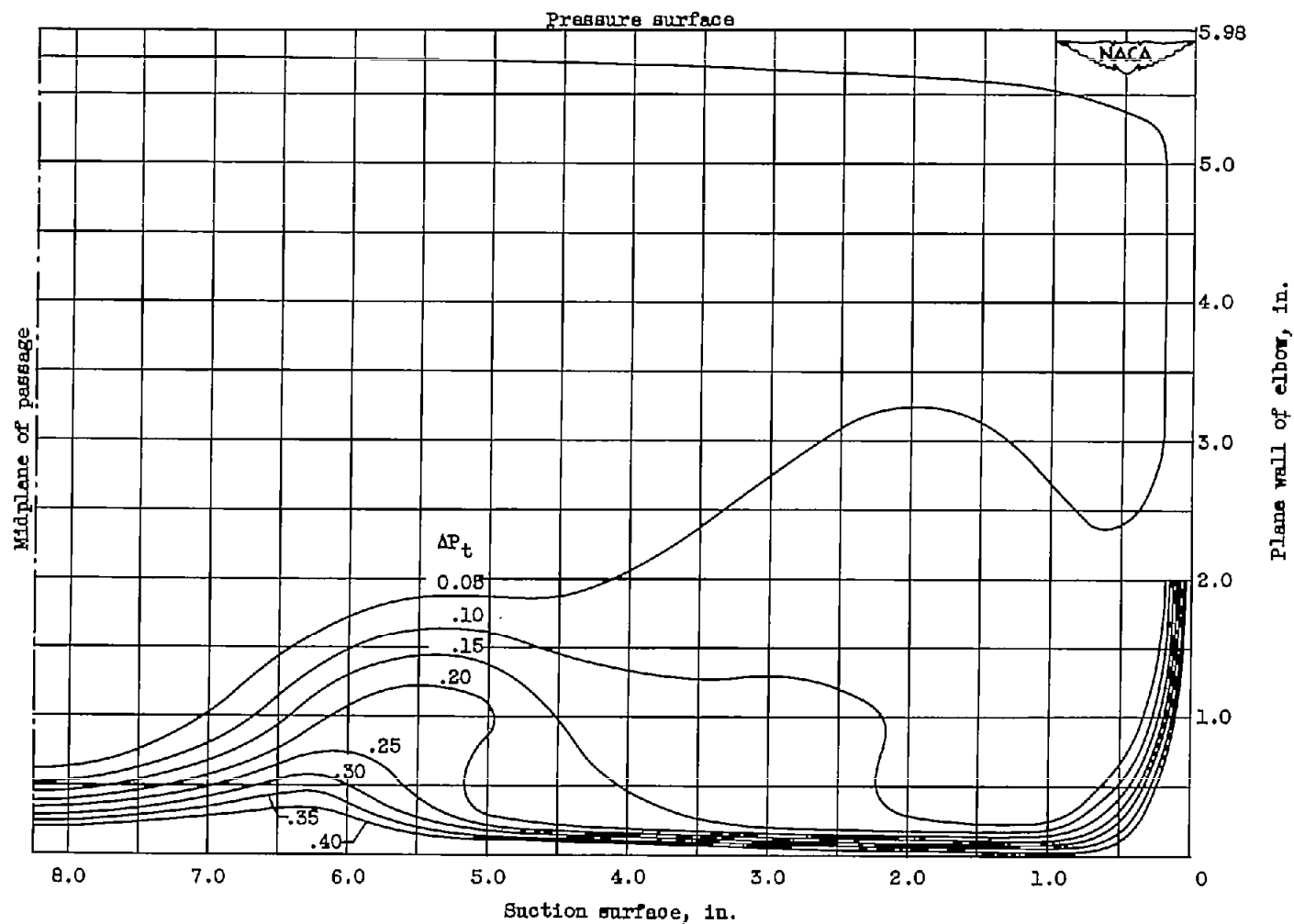
(a) No spoiler.

Figure 9. - Total-pressure-loss contours of constant ΔP_t in exit plane of 6-inch extension downstream of elbow. Exit Mach number, 0.4 (tank gage pressure ($p_T - p_a$), 46 in. water).



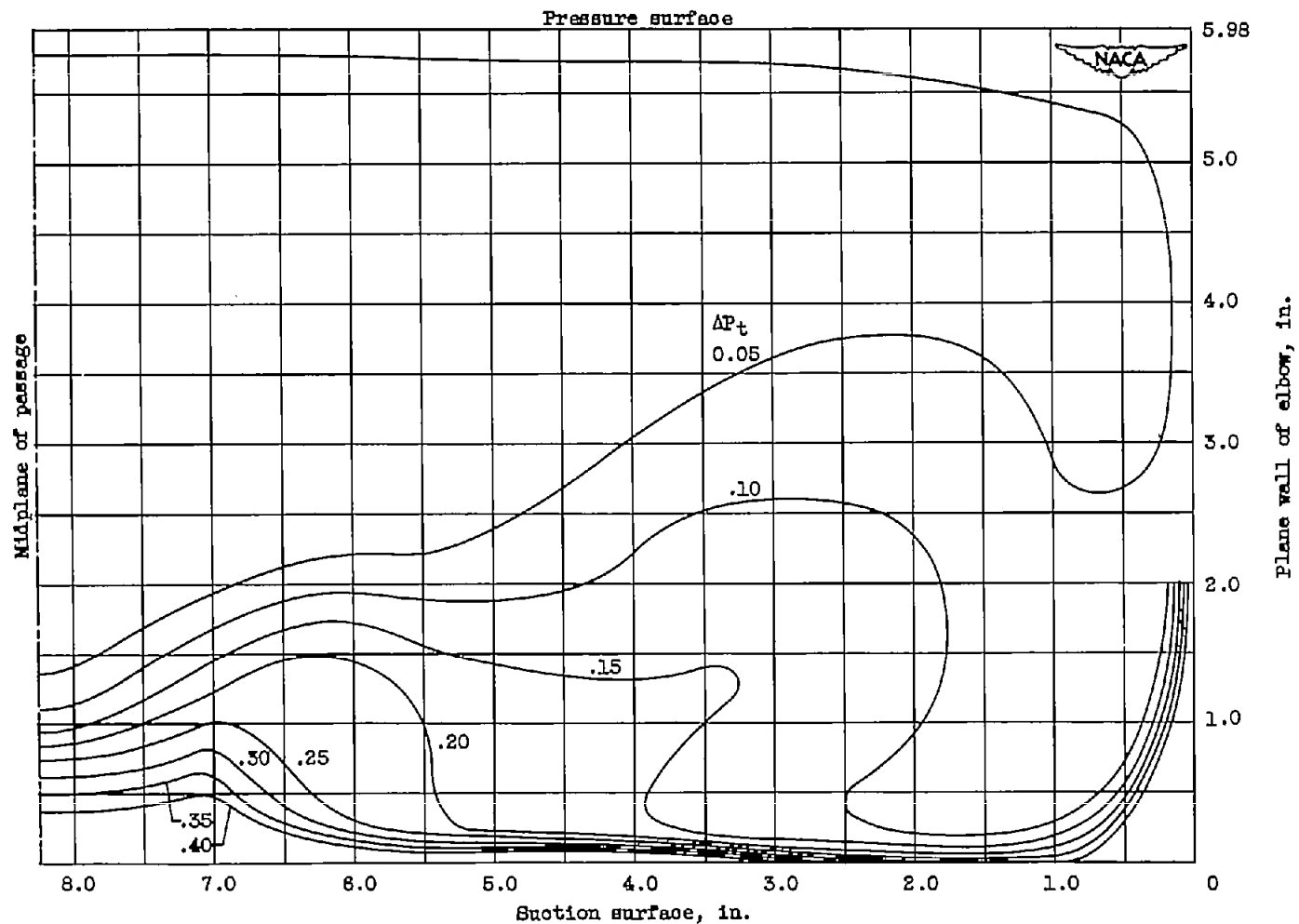
(b) 0.5-Inch spoiler.

Figure 9. - Continued. Total-pressure-loss contours of constant ΔP_t in exit plane of 6-inch extension downstream of elbow. Exit Mach number, 0.4 (tank gage pressure ($p_T - p_a$), 46 in. water).



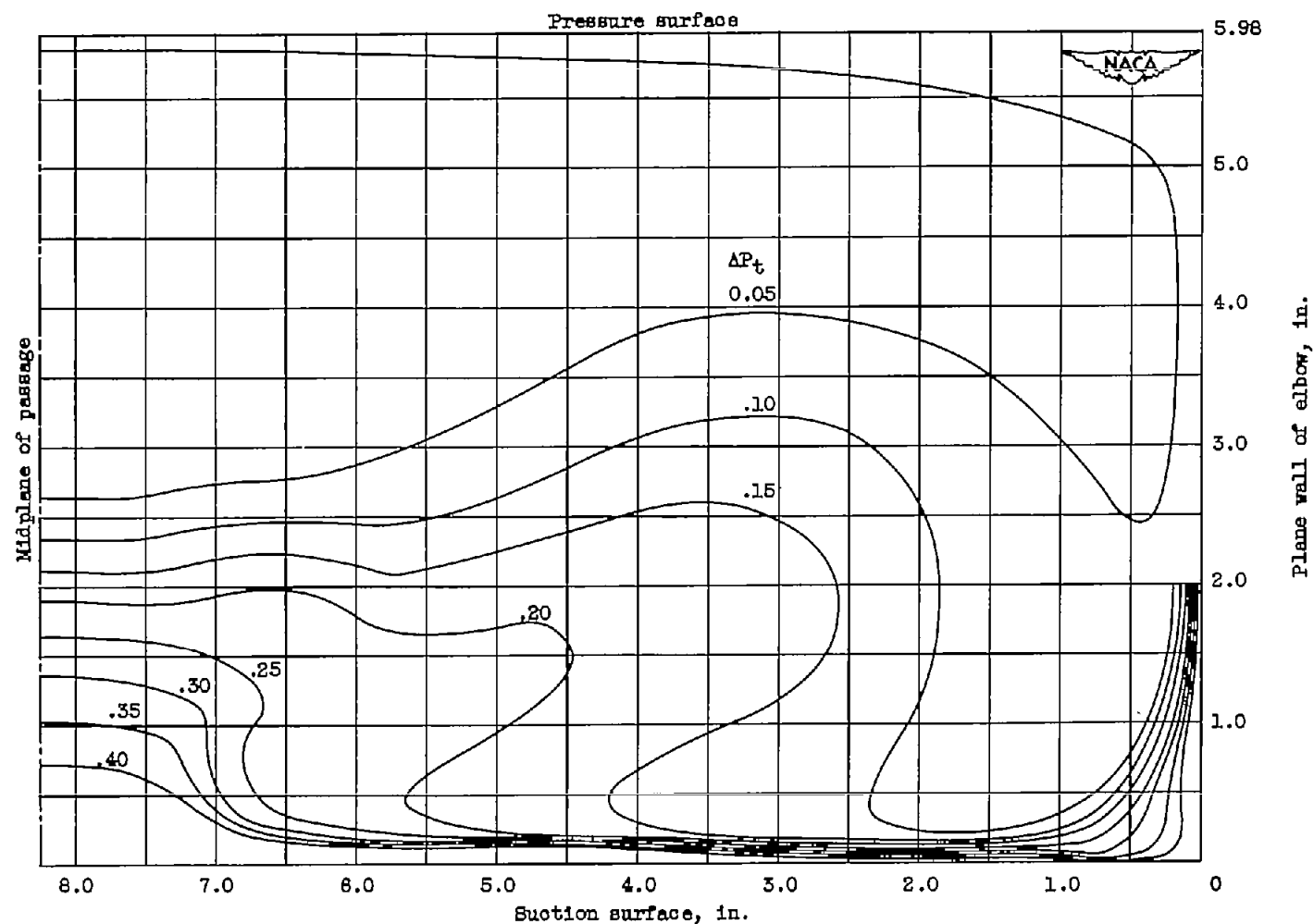
(a) 1.0-Inch spoiler.

Figure 8. - Continued. Total-pressure-loss contours of constant ΔP_t in exit plane of 6-inch extension downstream of elbow. Exit Mach number, 0.4 (tank gage pressure ($p_T - p_a$), 46 in. water).



(d) 1.5-Inch spoiler.

Figure 9. - Continued. Total-pressure-loss contours of constant ΔP_t in exit plane of 6-inch extension downstream of elbow. Exit Mach number, 0.4 (tank gage pressure ($p_T - p_a$), 46 in. water).



(e) 2.0-Inch spoiler.

Figure 9. - Continued. Total-pressure-loss contours of constant ΔP_t in exit plane of 6-inch extension downstream of elbow. Exit Mach number, 0.4 (tank gage pressure ($P_T - P_a$), 45 in. water).

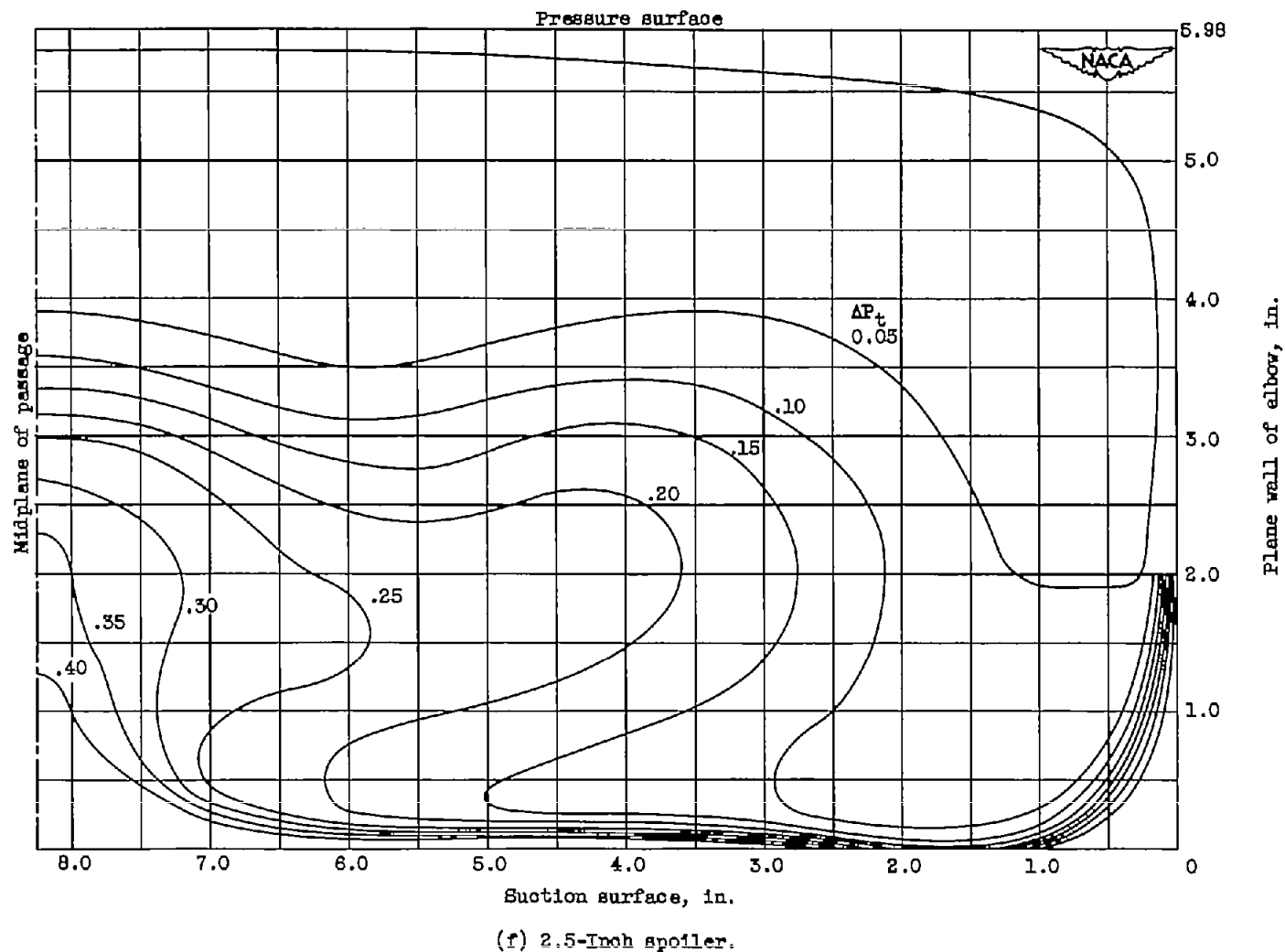


Figure 9. - Concluded. Total-pressure-loss contours of constant ΔP_t in exit plane of 6-inch extension downstream of elbow. Exit Mach number, 0.4 (tank gage pressure ($p_T - p_a$), 46 in. water).

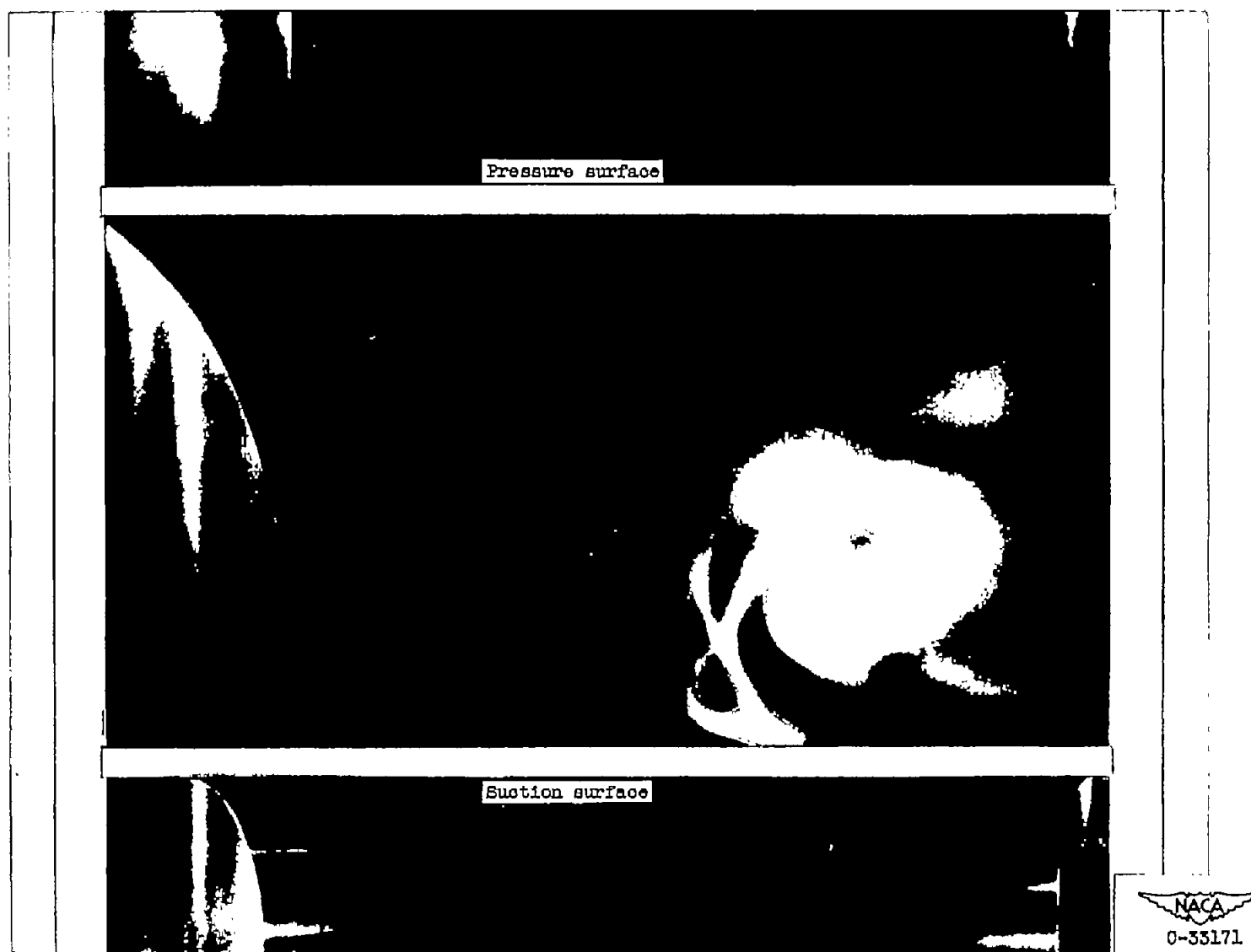


Figure 10. - Smoke trace showing formation of passage vortex (at elbow exit). Smoke injected into boundary layer (at elbow inlet) on plane wall of elbow of smaller Lucite model. (Elbow walls retouched for clarity.)

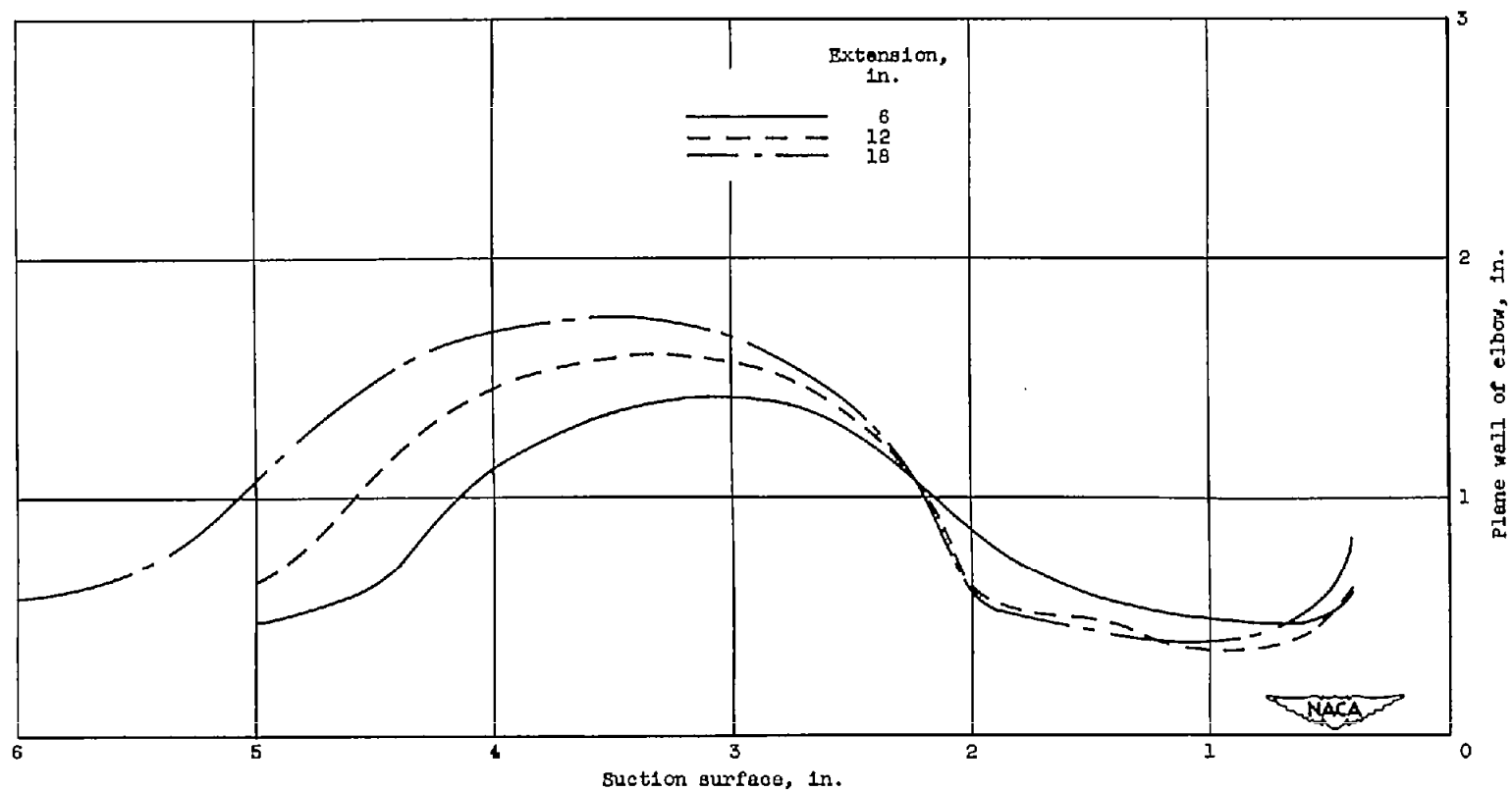
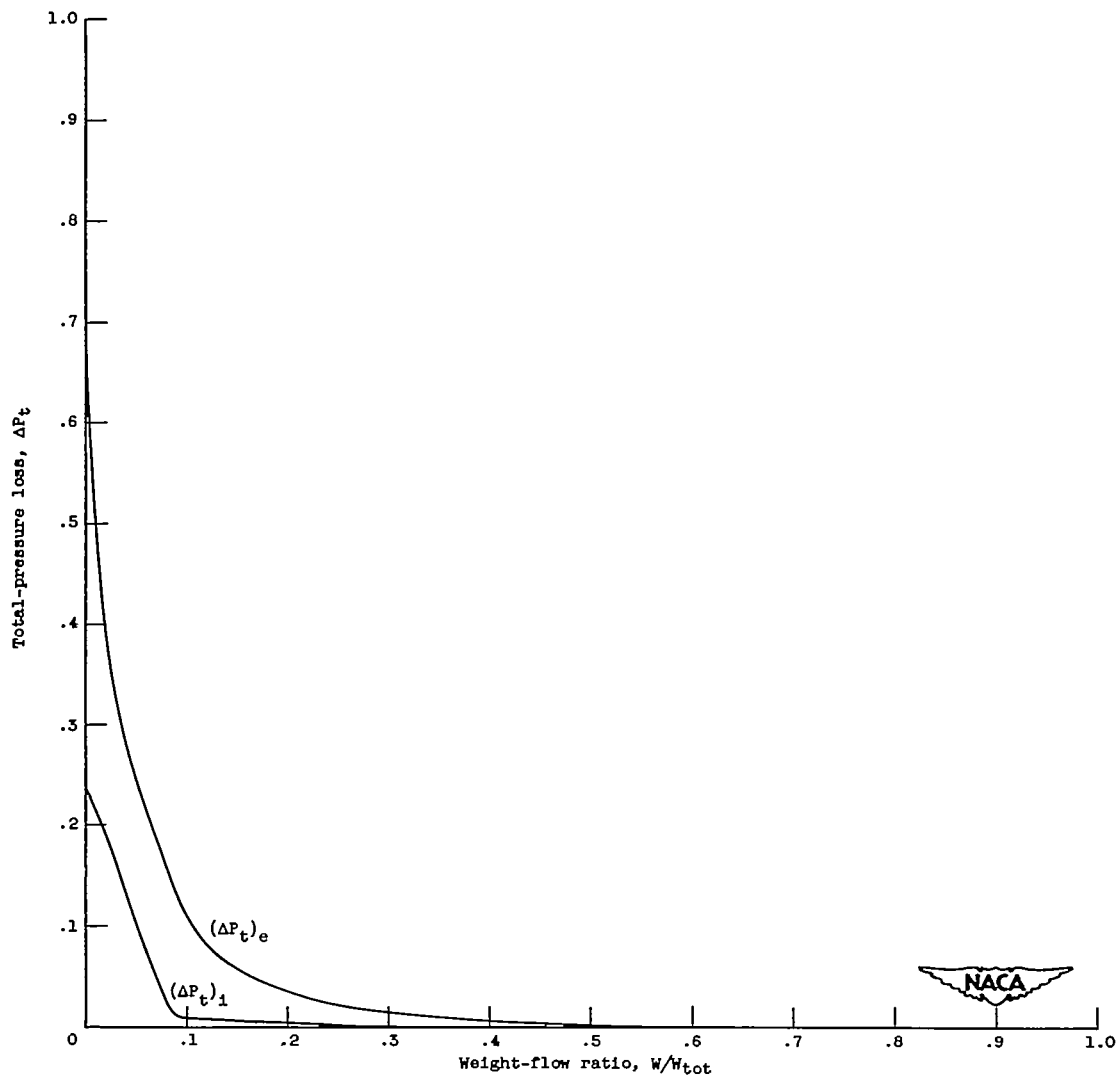


Figure 11. - Location of 0.05 total-pressure-loss contour in exit planes of 6-, 12-, and 18-inch extensions downstream of elbow. Exit Mach number, 0.4 (tank gage pressure ($p_T - p_B$), 46 in. water); no spoiler.

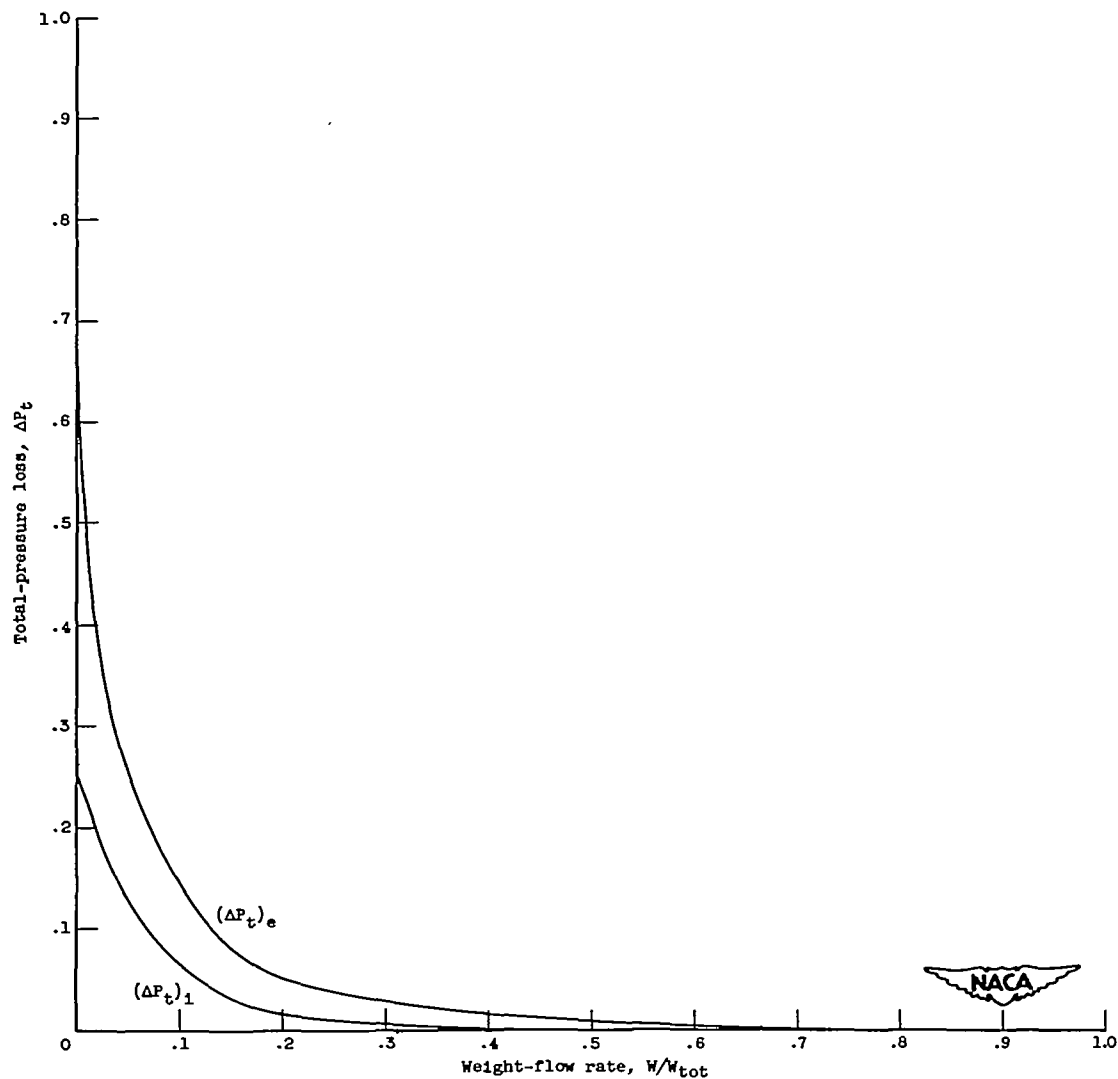
3005

CY-6 back



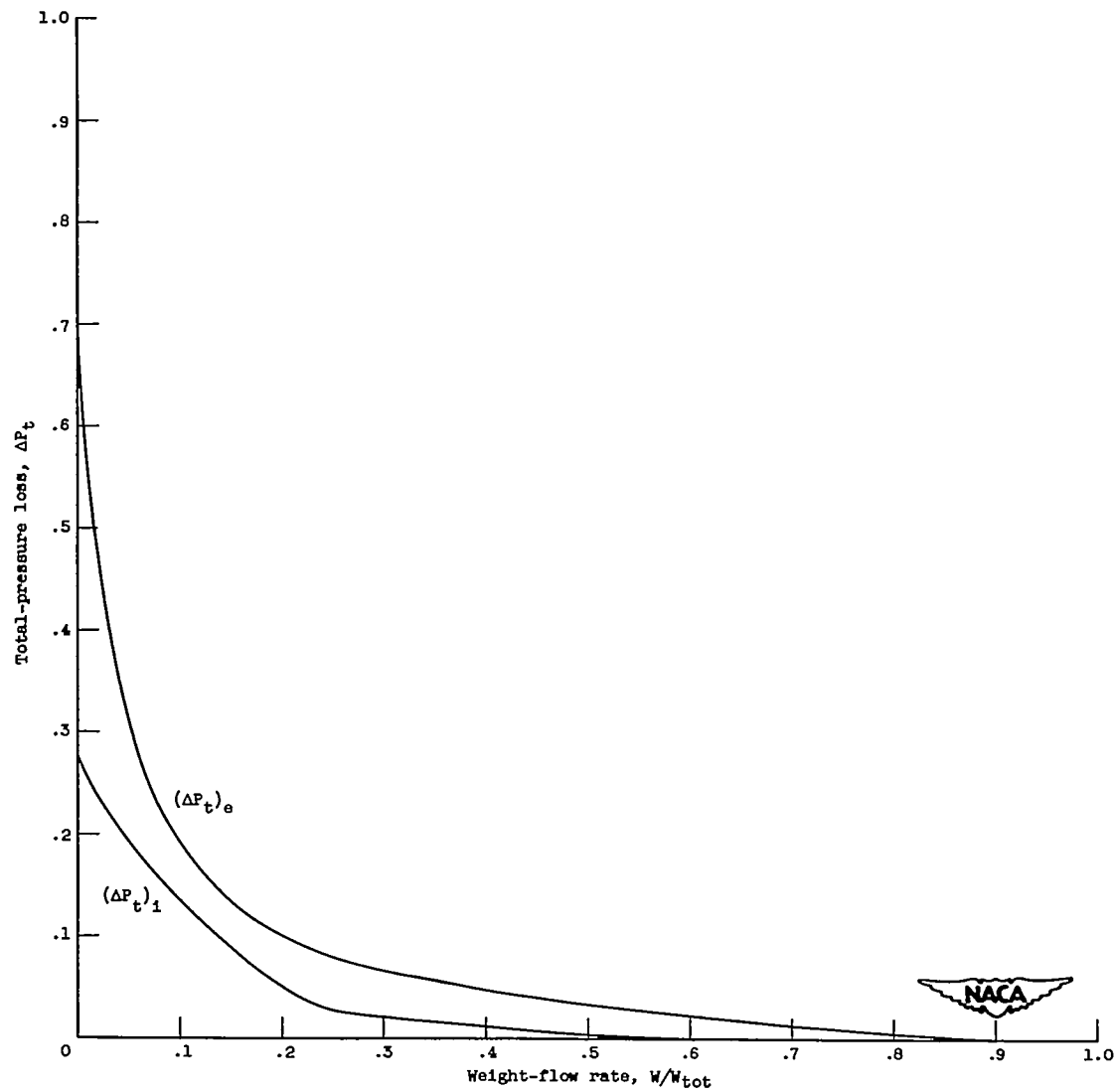
(a) No spoiler.

Figure 12. - Variation in total-pressure loss ΔP_t at inlet and exit planes of elbow as a function of weight-flow ratio W/W_{tot} where, for each value of ΔP_t , W/W_{tot} is percent of total weight-flow rate that has a total-pressure loss at least as high as ΔP_t .



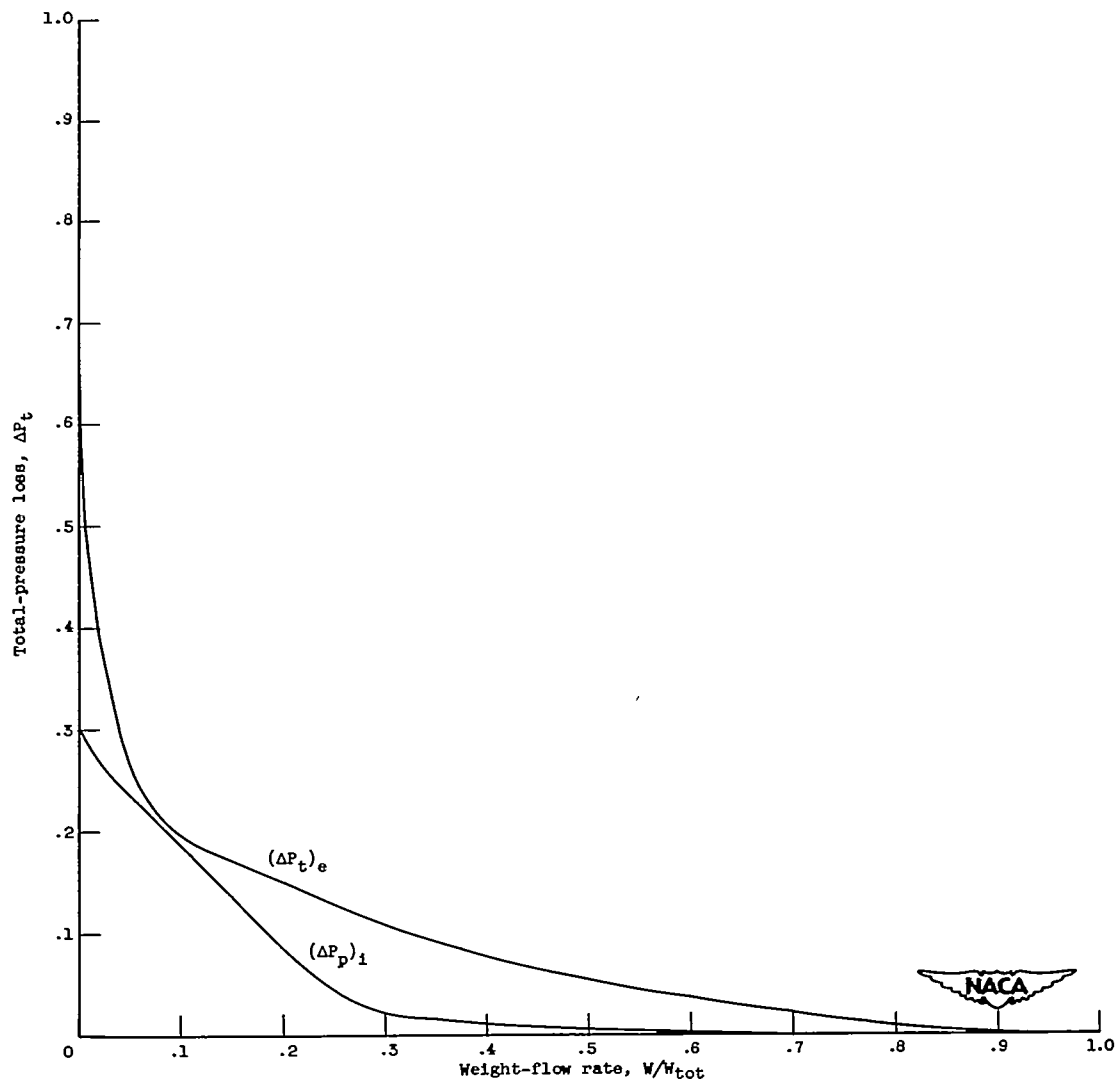
(b) 0.5-Inch spoiler.

Figure 12. - Continued. Variation in total-pressure loss ΔP_t at inlet and exit planes of elbow as a function of weight-flow ratio W/W_{tot} where, for each value of ΔP_t , W/W_{tot} is percent of total weight-flow rate that has a total-pressure loss at least as high as ΔP_t .



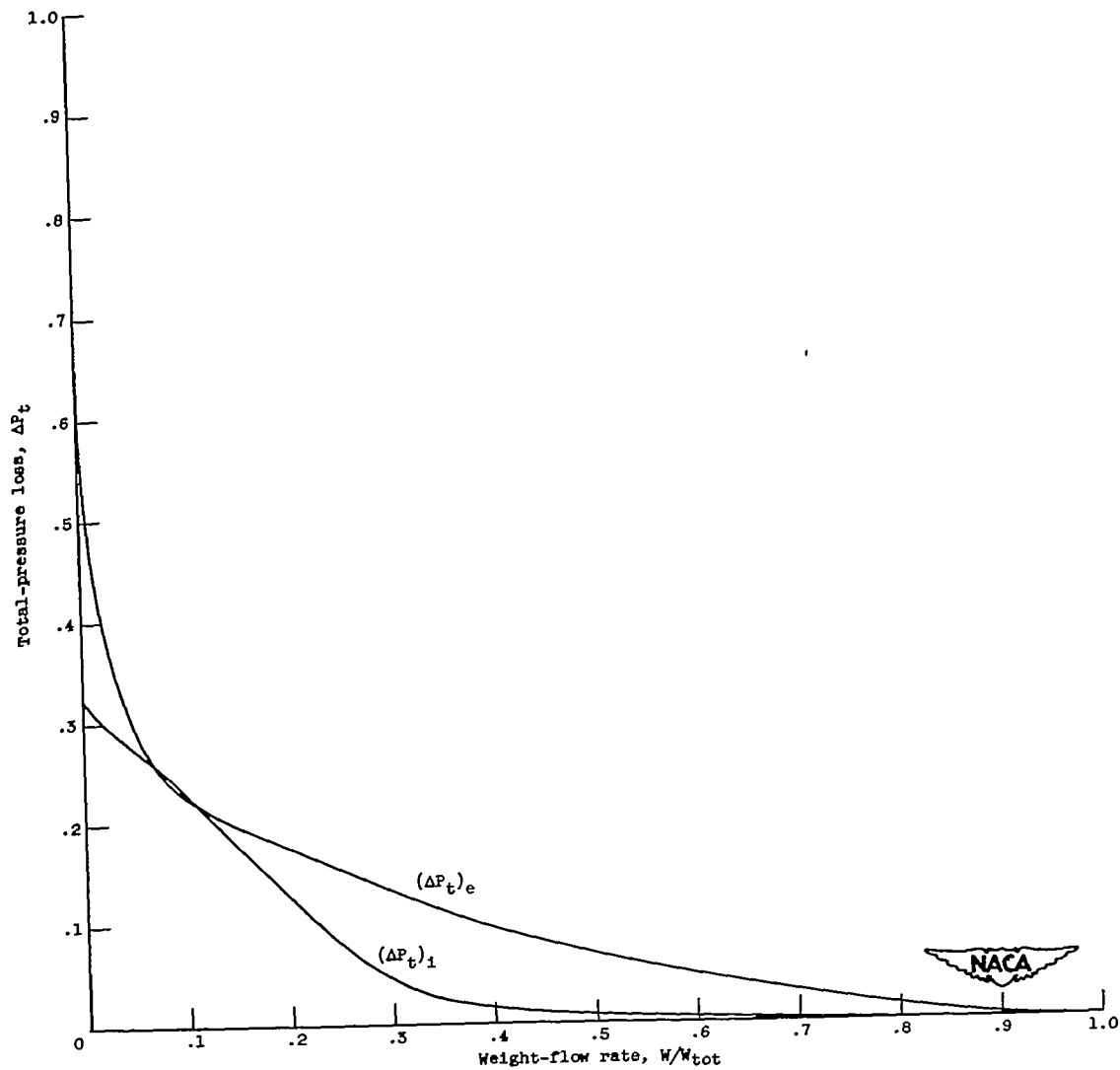
(c) 1.0-Inch spoiler.

Figure 12. - Continued. Variation in total-pressure loss ΔP_t at inlet and exit planes of elbow as a function of weight-flow ratio W/W_{tot} where, for each value of ΔP_t , W/W_{tot} is percent of total weight-flow rate that has a total-pressure loss at least as high as ΔP_t .



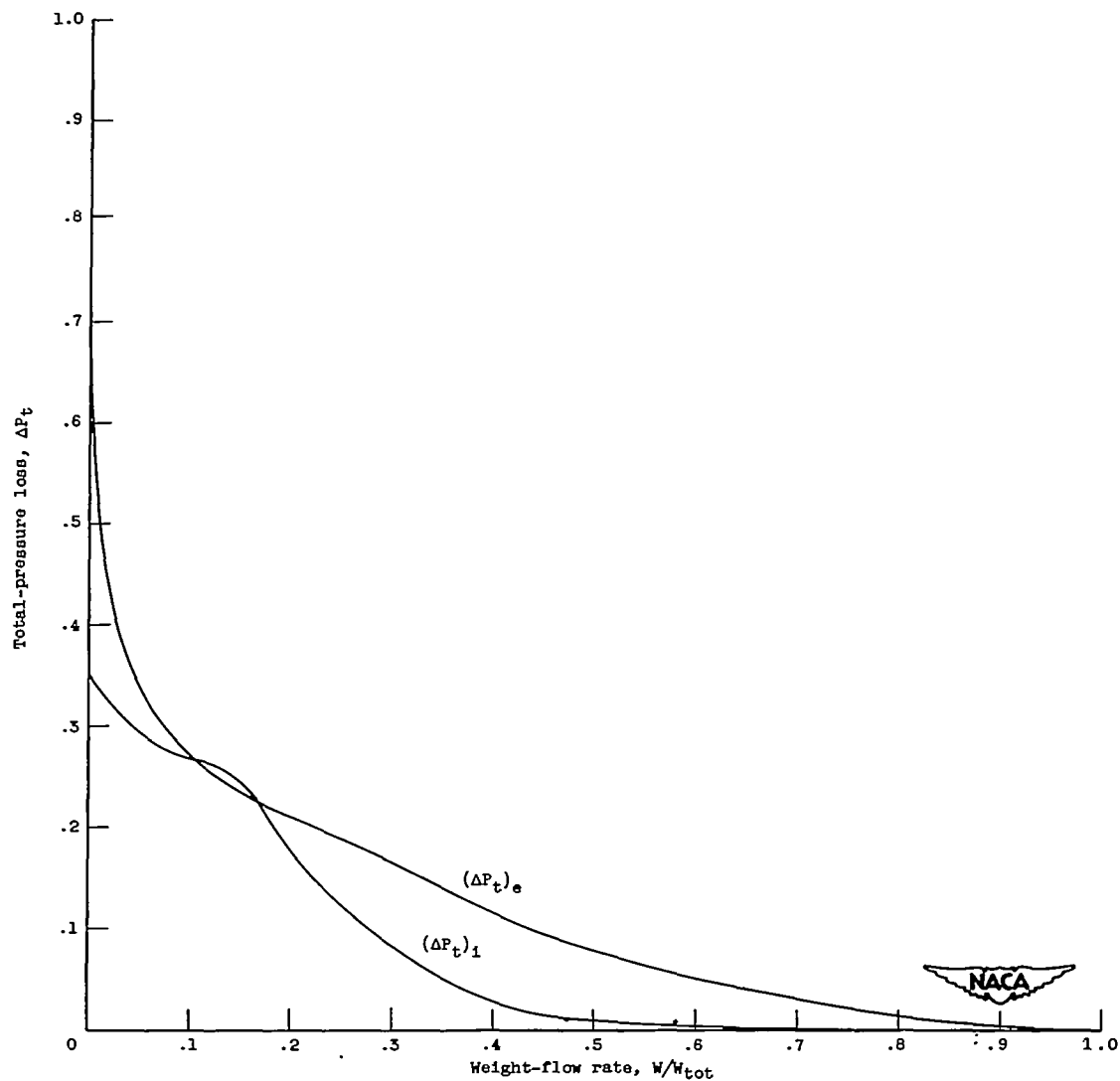
(d) 1.5-Inch spoiler.

Figure 12. - Continued. Variation in total-pressure loss ΔP_t at inlet and exit planes of elbow as a function of weight-flow ratio W/W_{tot} where, for each value of ΔP_t , W/W_{tot} is percent of total weight-flow rate that has a total-pressure loss at least as high as ΔP_t .



(e) 2.0-Inch spoiler.

Figure 12. - Continued. Variation in total-pressure loss ΔP_t at inlet and exit planes of elbow as a function of weight-flow ratio W/W_{tot} where, for each value of ΔP_t , W/W_{tot} is percent of total weight-flow rate that has a total-pressure loss at least as high as ΔP_t .



(f) 2.5-Inch spoiler.

Figure 12. - Concluded. Variation in total-pressure loss ΔP_t at inlet and exit planes of elbow as a function of weight-flow ratio W/W_{tot} where, for each value of ΔP_t , W/W_{tot} is percent of total weight-flow rate that has a total-pressure loss at least as high as ΔP_t .

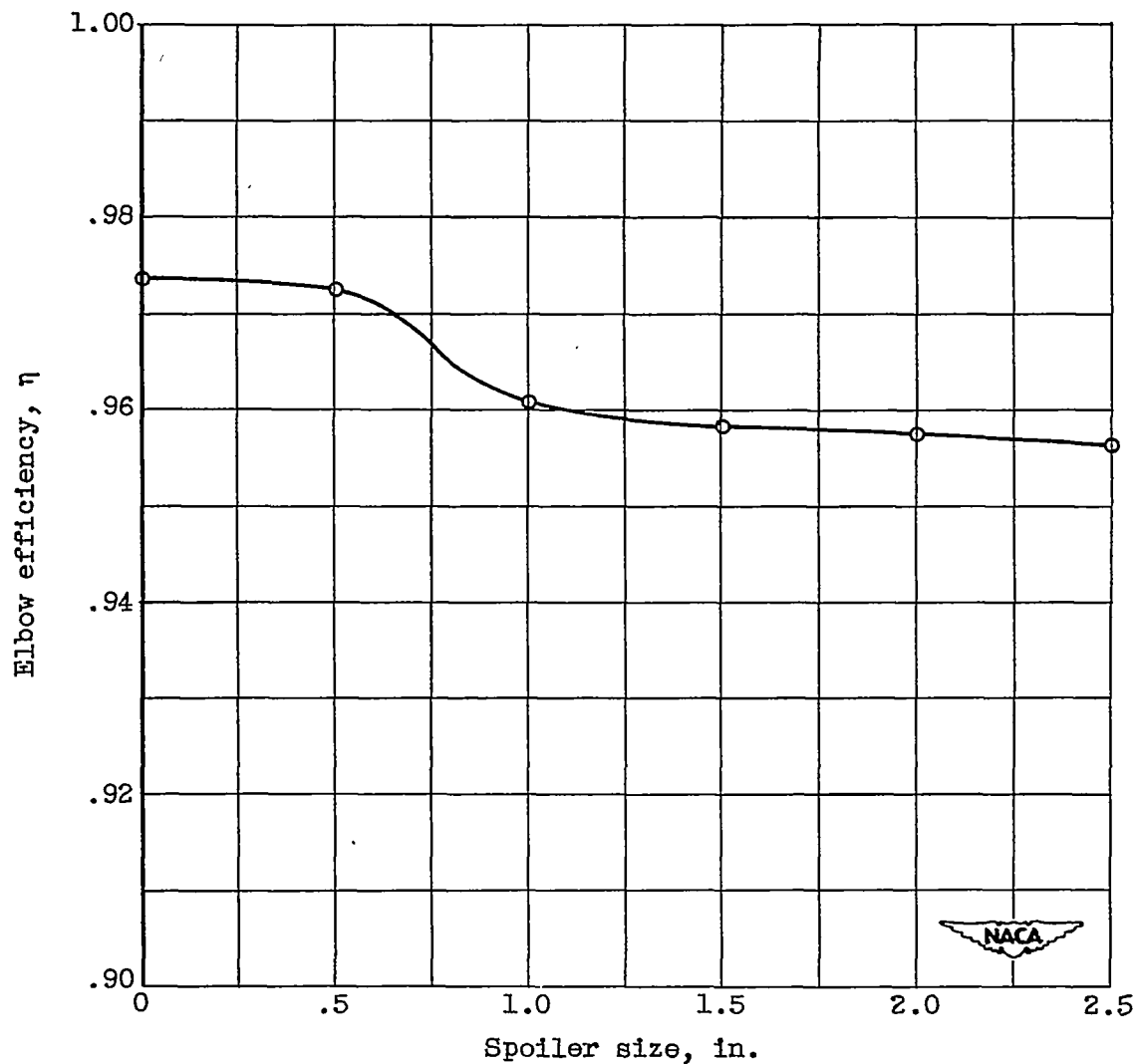


Figure 13. - Variation in elbow efficiency with spoiler size.
Equation (2).

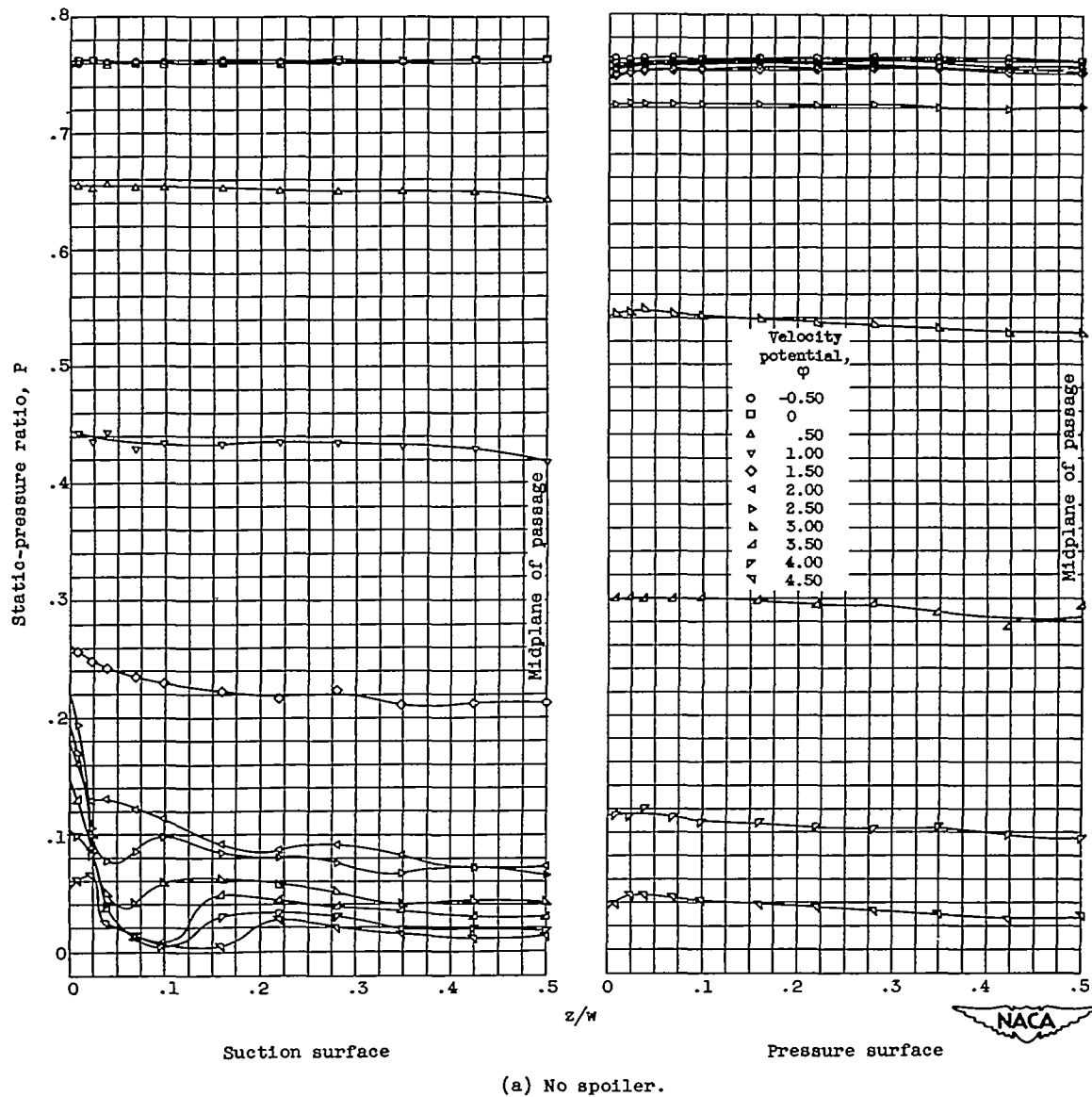
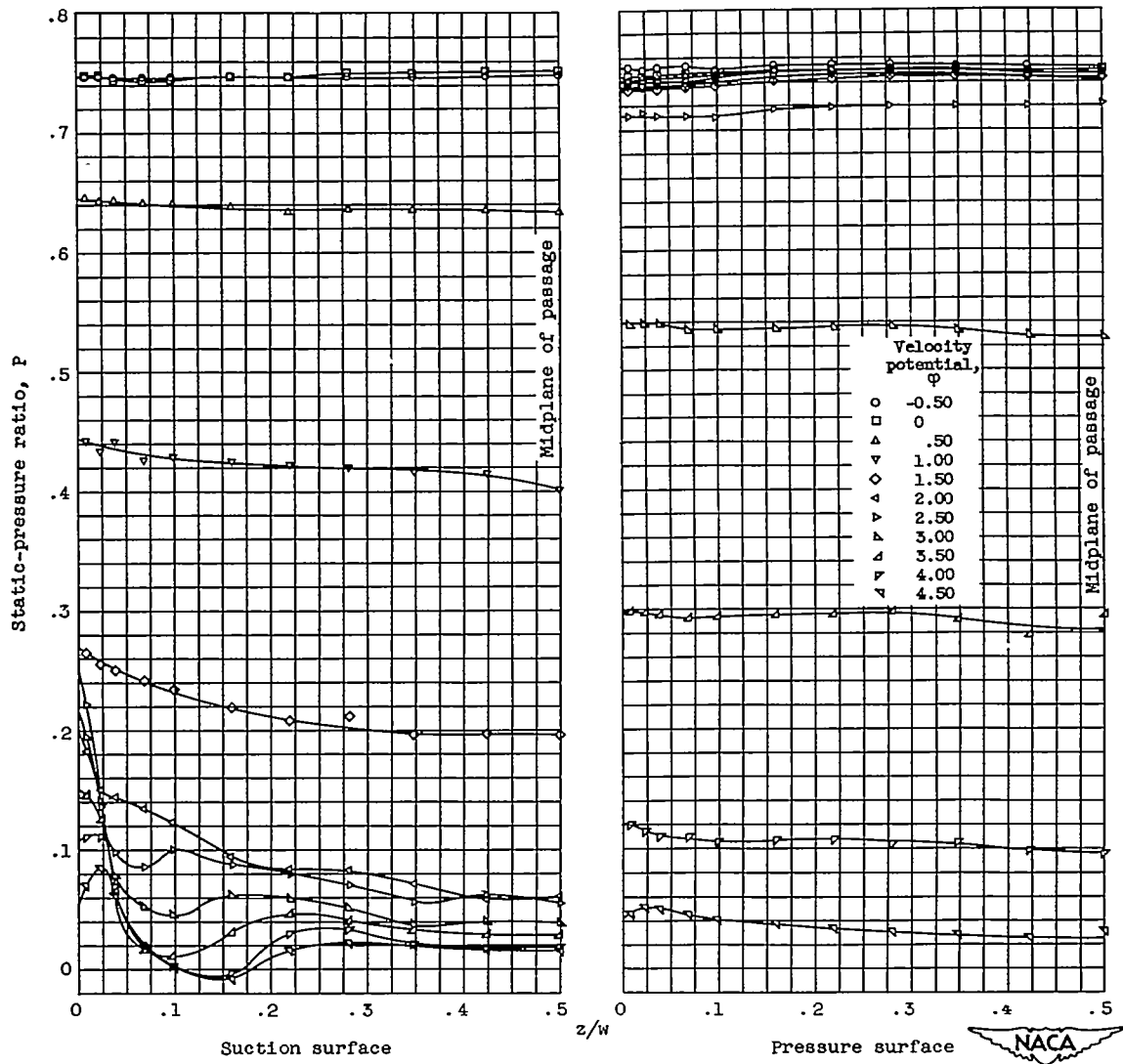


Figure 14. - Spanwise distribution of static pressure on pressure and suction surfaces of elbow. Tank gage pressure ($P_T - P_a$), 20 inches of water.

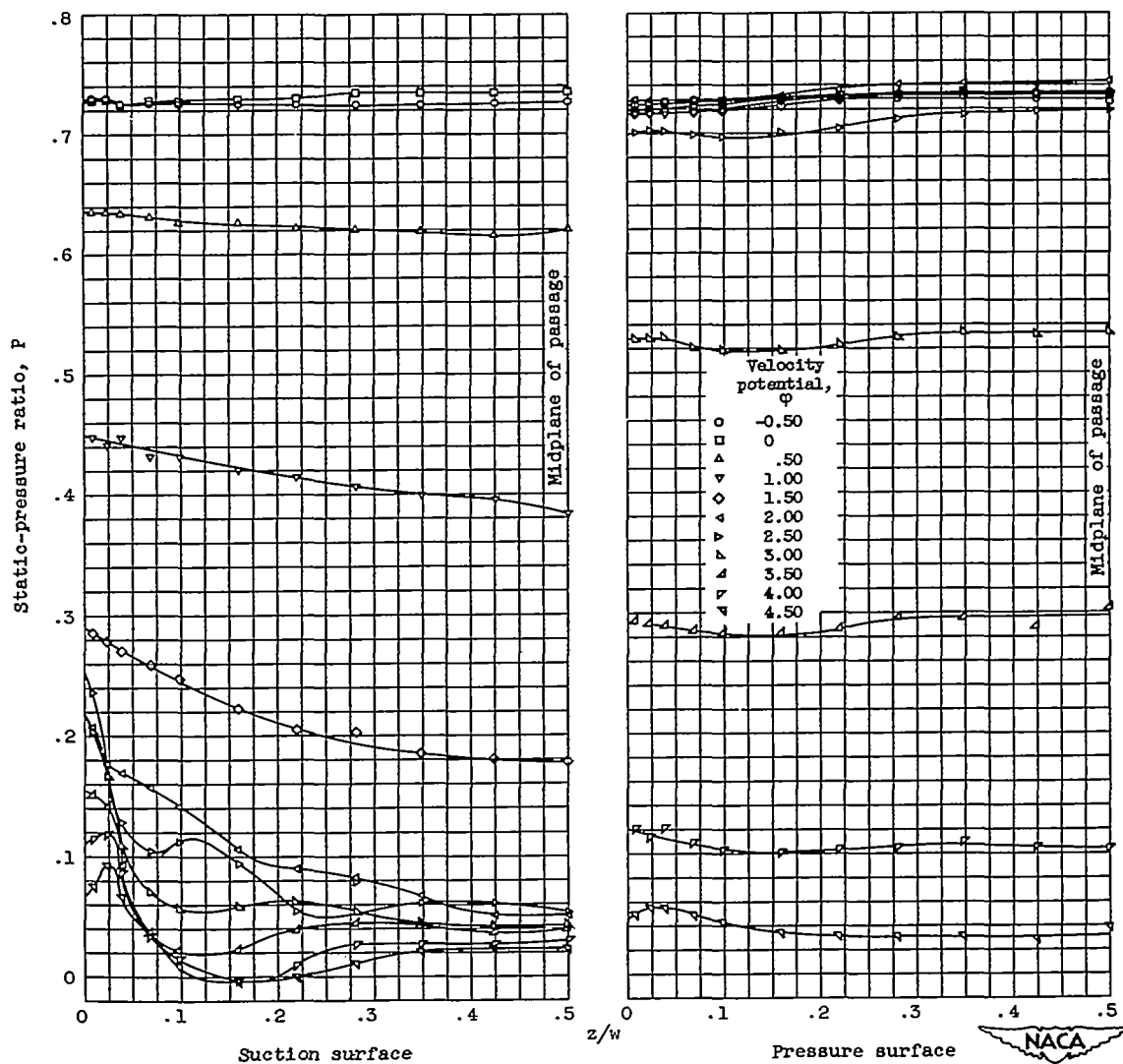
3005

CY-7 back



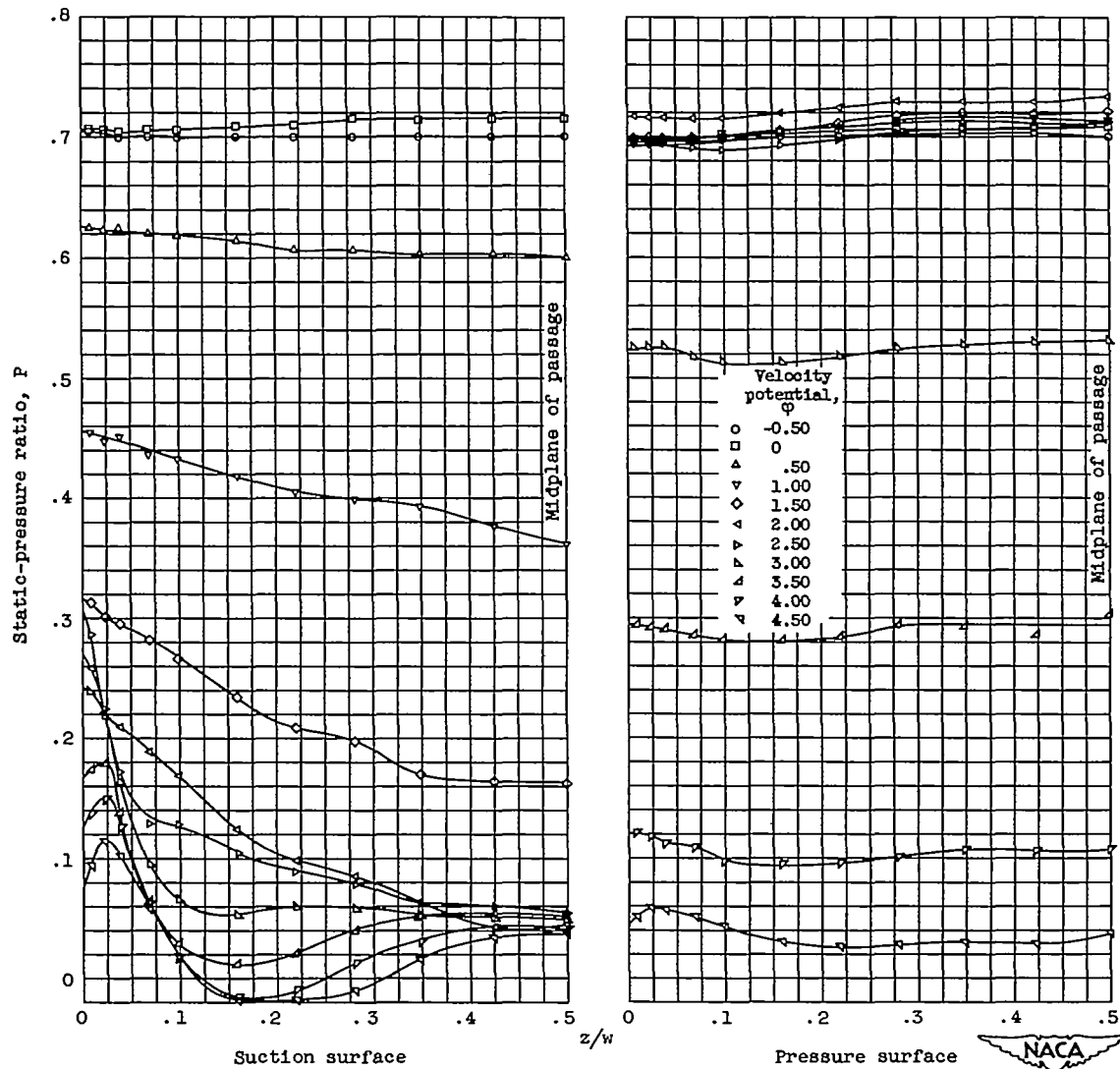
(b) 0.5-Inch spoiler.

Figure 14. - Continued. Spanwise distribution of static pressure on pressure and suction surfaces of elbow. Tank gage pressure ($p_T - p_a$), 20 inches of water.



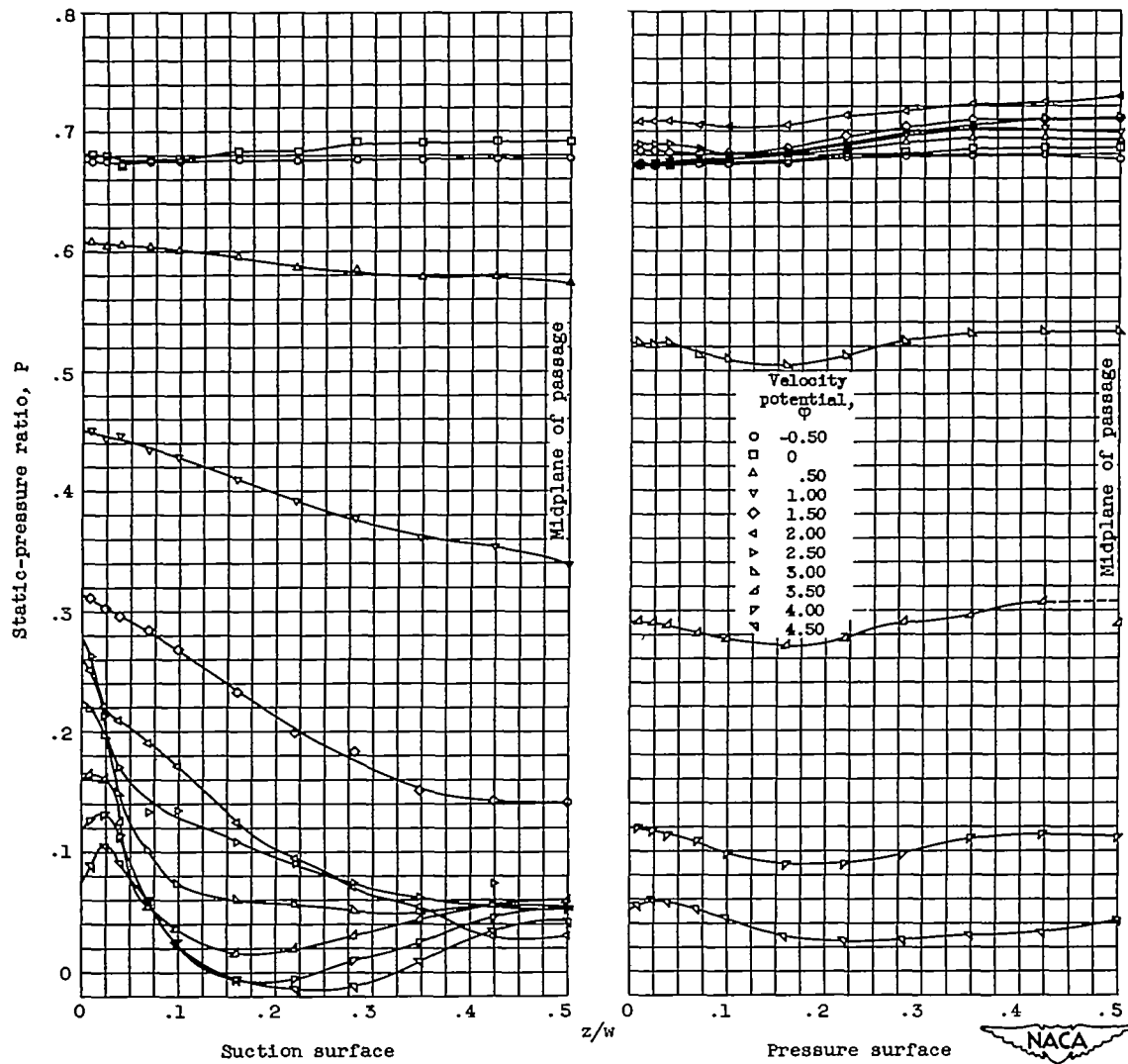
(c) 1.0-Inch spoiler.

Figure 14. - Continued. Spanwise distribution of static pressure on pressure and suction surfaces of elbow. Tank gage pressure ($p_T - p_a$), 20 inches of water.



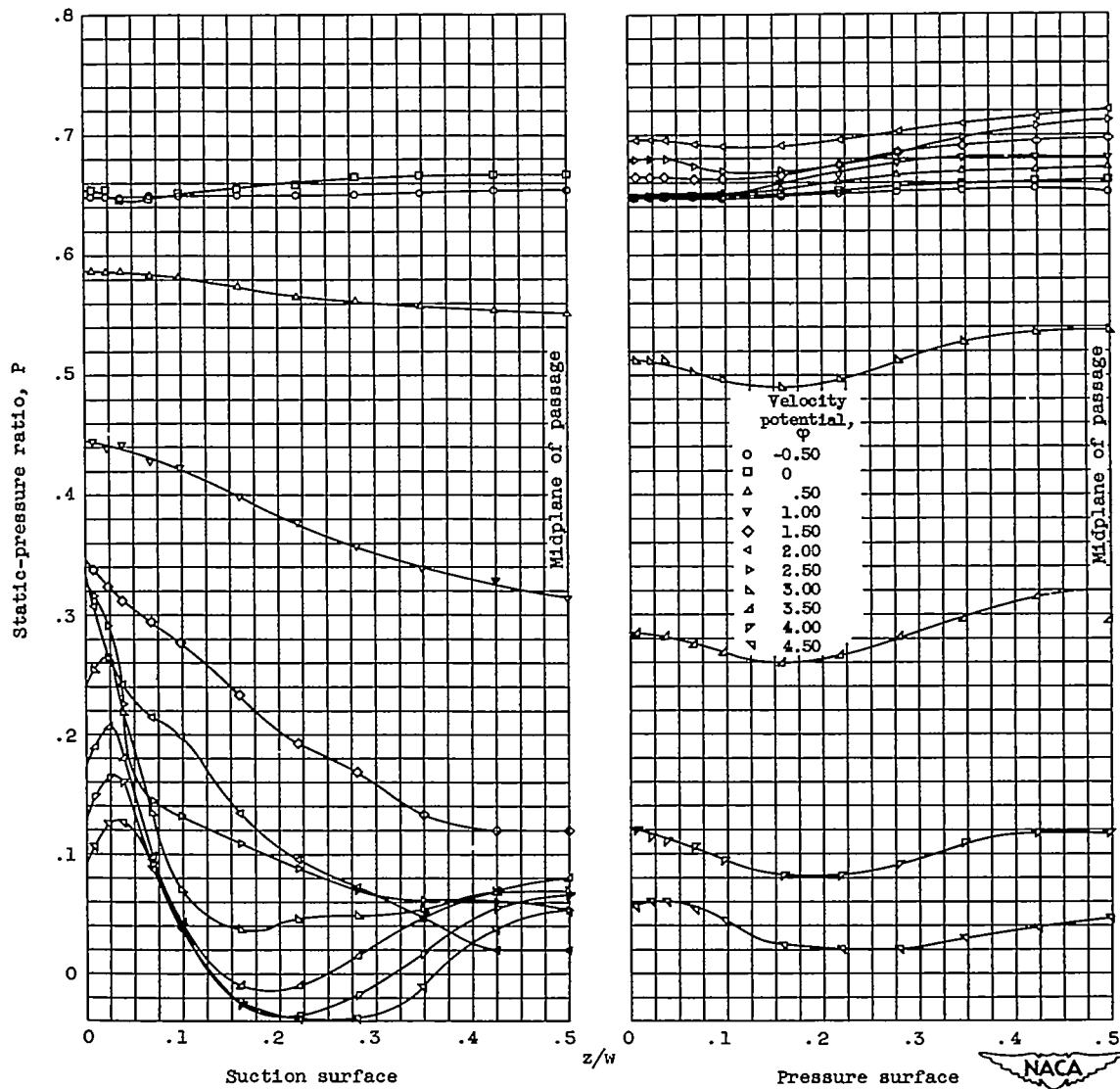
(d) 1.5-Inch spoiler.

Figure 14. - Continued. Spanwise distribution of static pressure on pressure and suction surfaces of elbow. Tank gage pressure ($p_T - p_a$), 20 inches of water.



(e) 2.0-Inch spoiler.

Figure 14. - Continued. Spanwise distribution of static pressure on pressure and suction surfaces of elbow. Tank gage pressure ($p_T - p_a$), 20 inches of water.



(f) 2.5-Inch spoiler.

Figure 14. - Concluded. Spanwise distribution of static pressure on pressure and suction surfaces of elbow. Tank gage pressure ($p_T - p_a$) 20 inches of water.

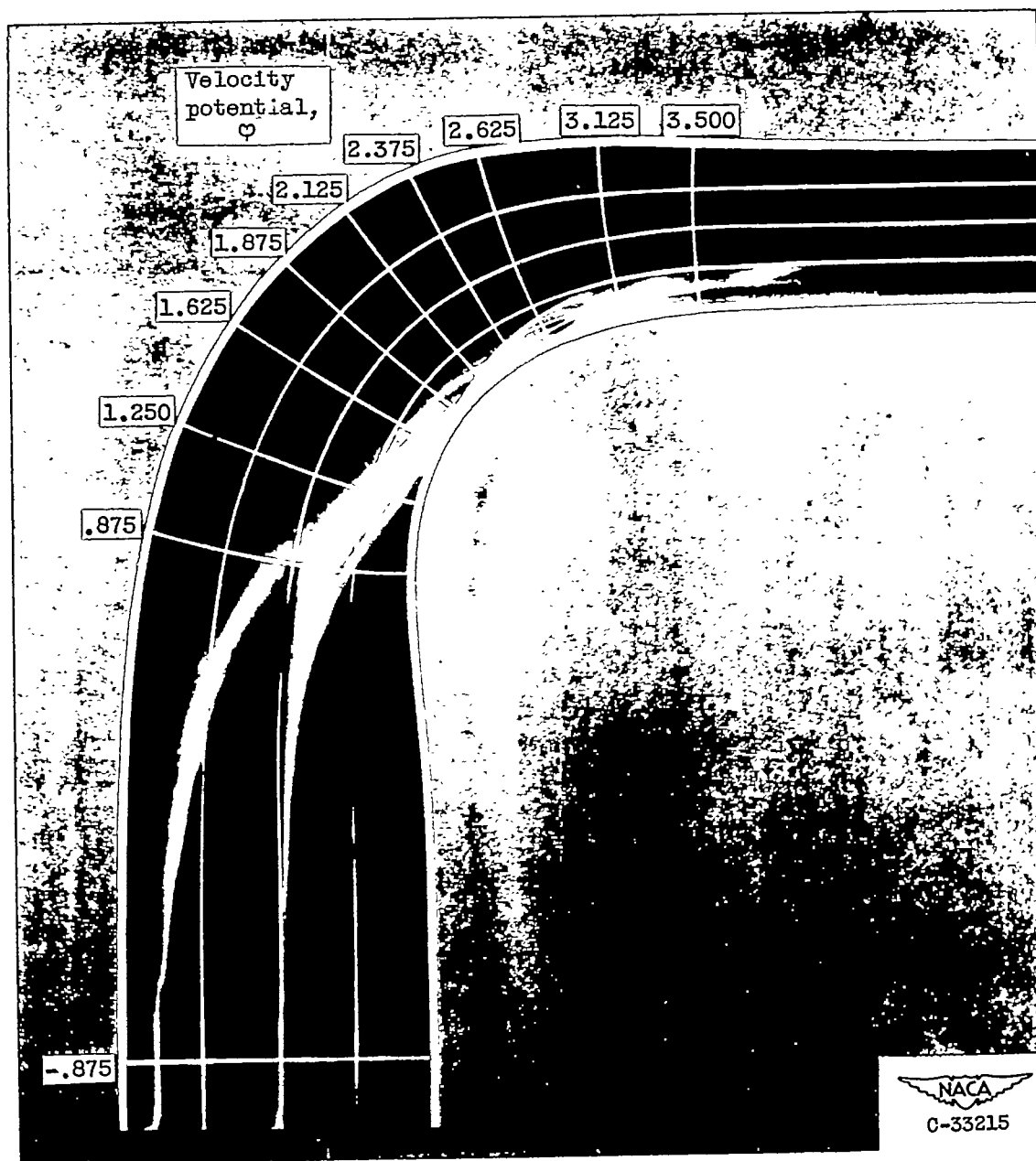


Figure 15. - Smoke traces showing convergence of secondary (boundary-layer) flow to suction surface of elbow at values of ϕ between 1.5 and 2.0. Smoke injected into boundary layer close to plane wall of elbow, in smaller Lucite model.

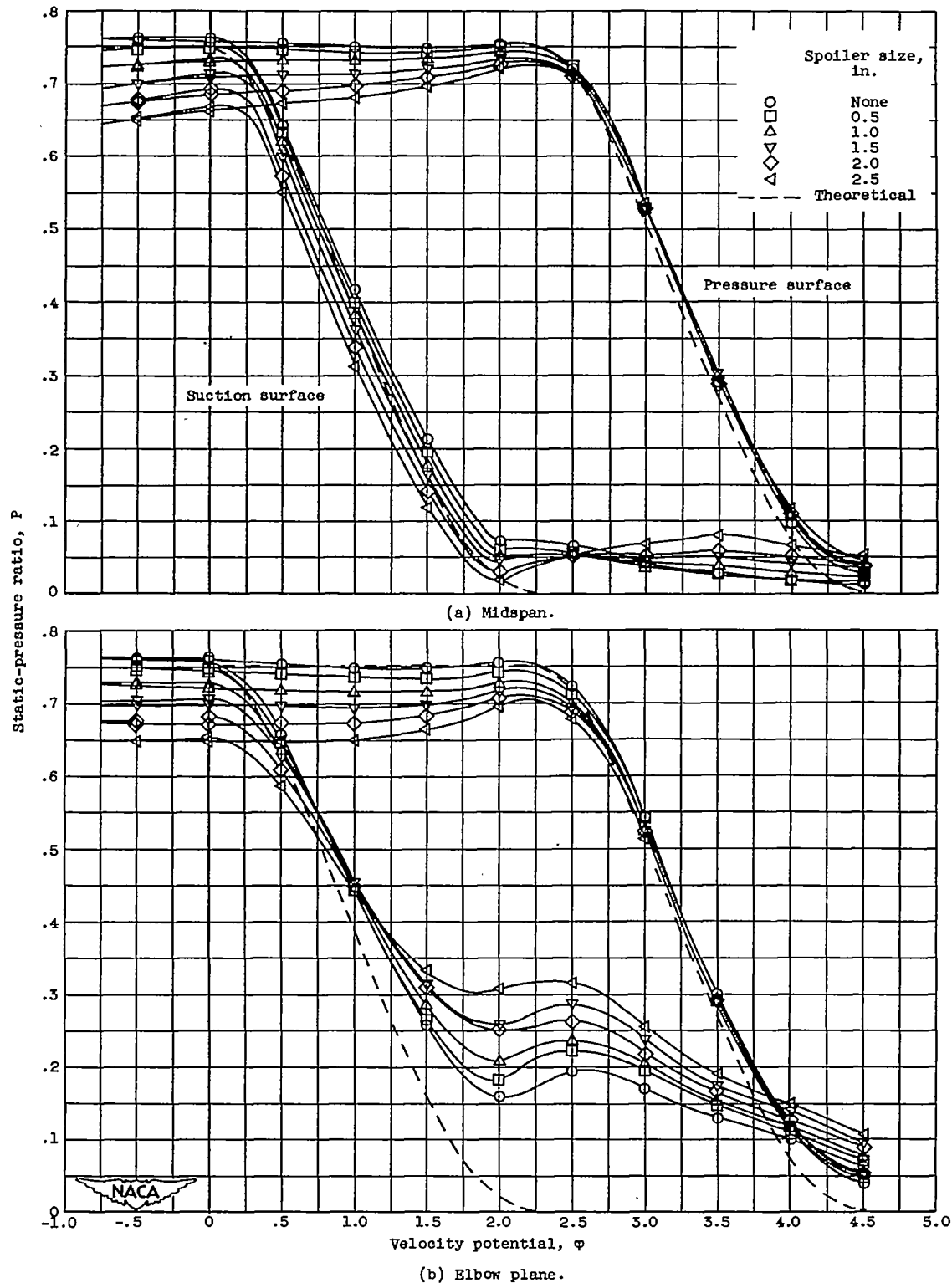


Figure 16. - Theoretical and experimental variations in static pressure with velocity potential along elbow profile. Velocity potential is related to channel shape in figure 5 and table I.

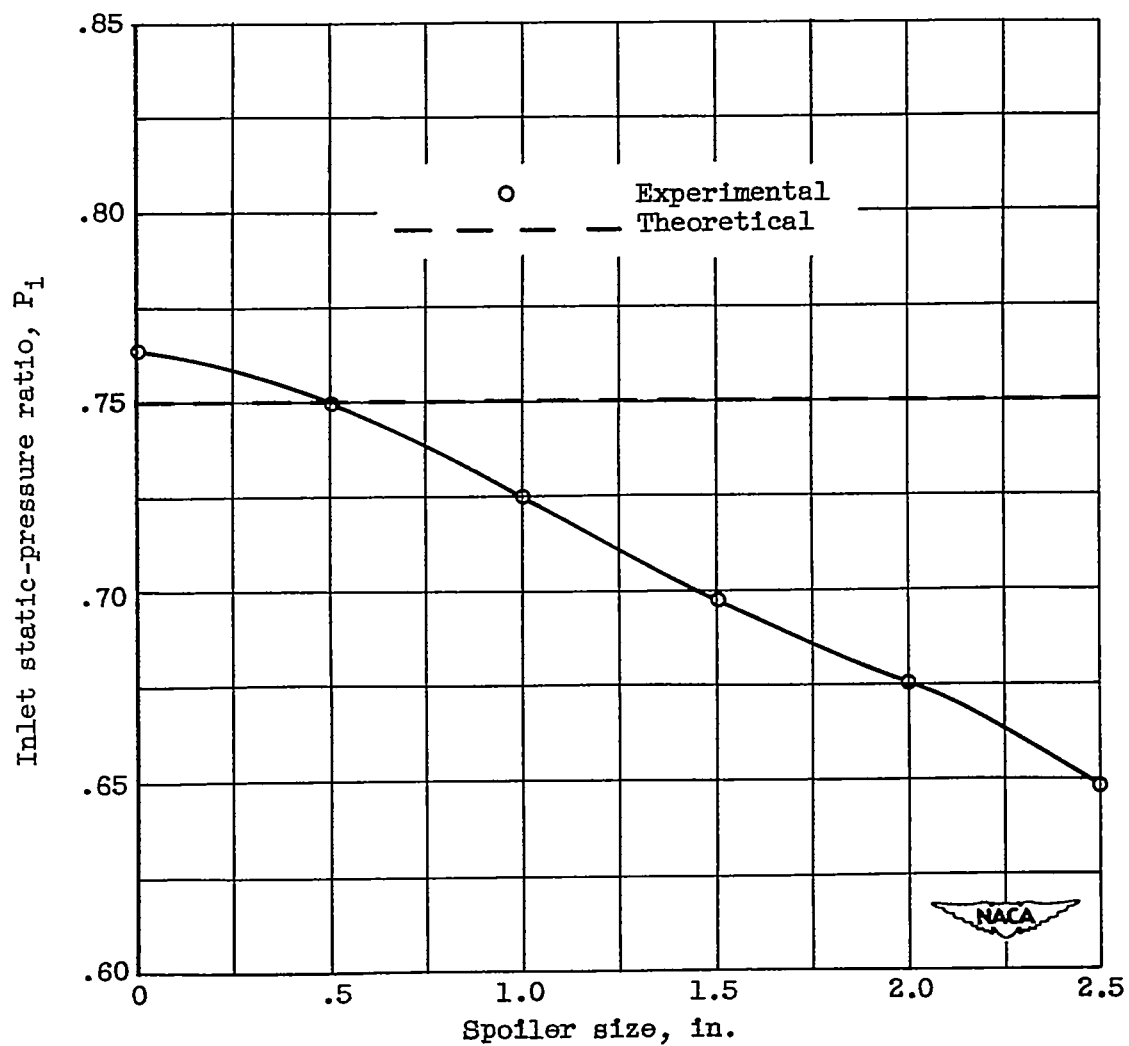


Figure 17. - Variation in inlet static pressure with spoiler size. Tank gage pressure ($p_T - p_a$), 20 inches of water.

3005

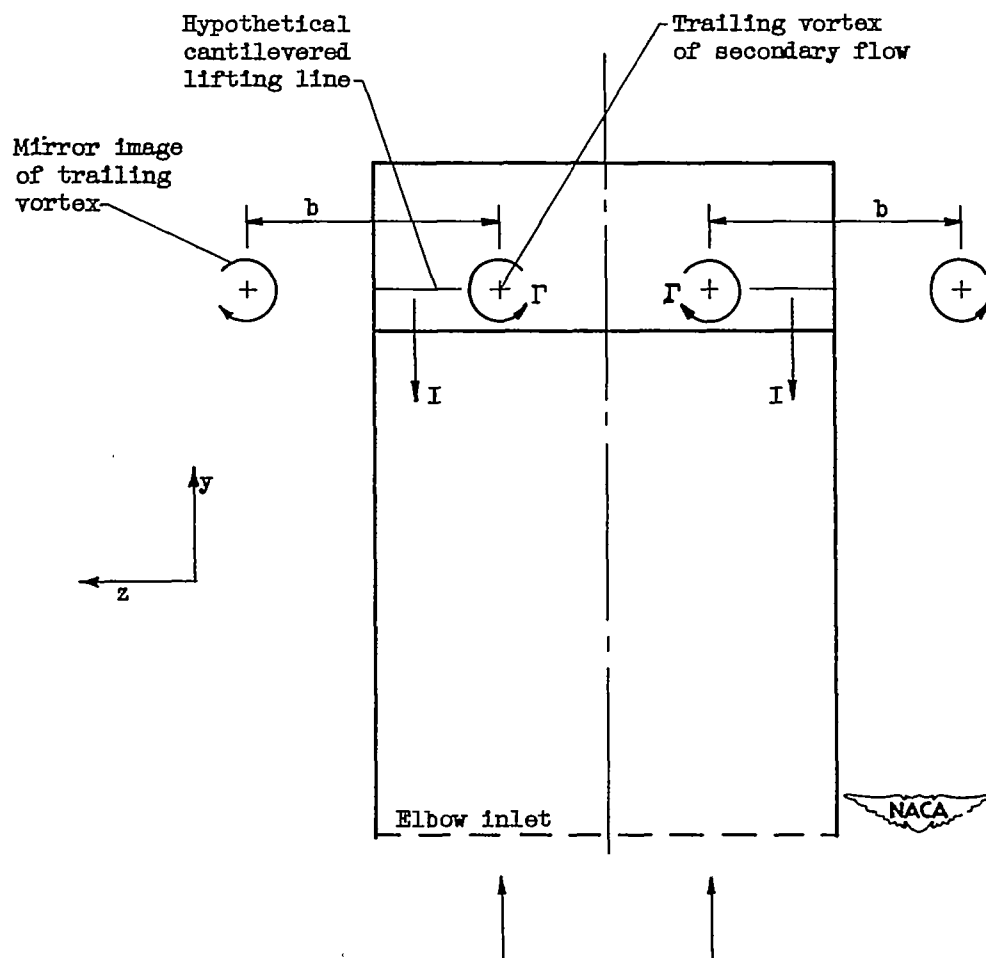


Figure 18. - Hypothetical cantilevered lifting line and trailing vortices (with images) of secondary flow in exit plane of elbow.

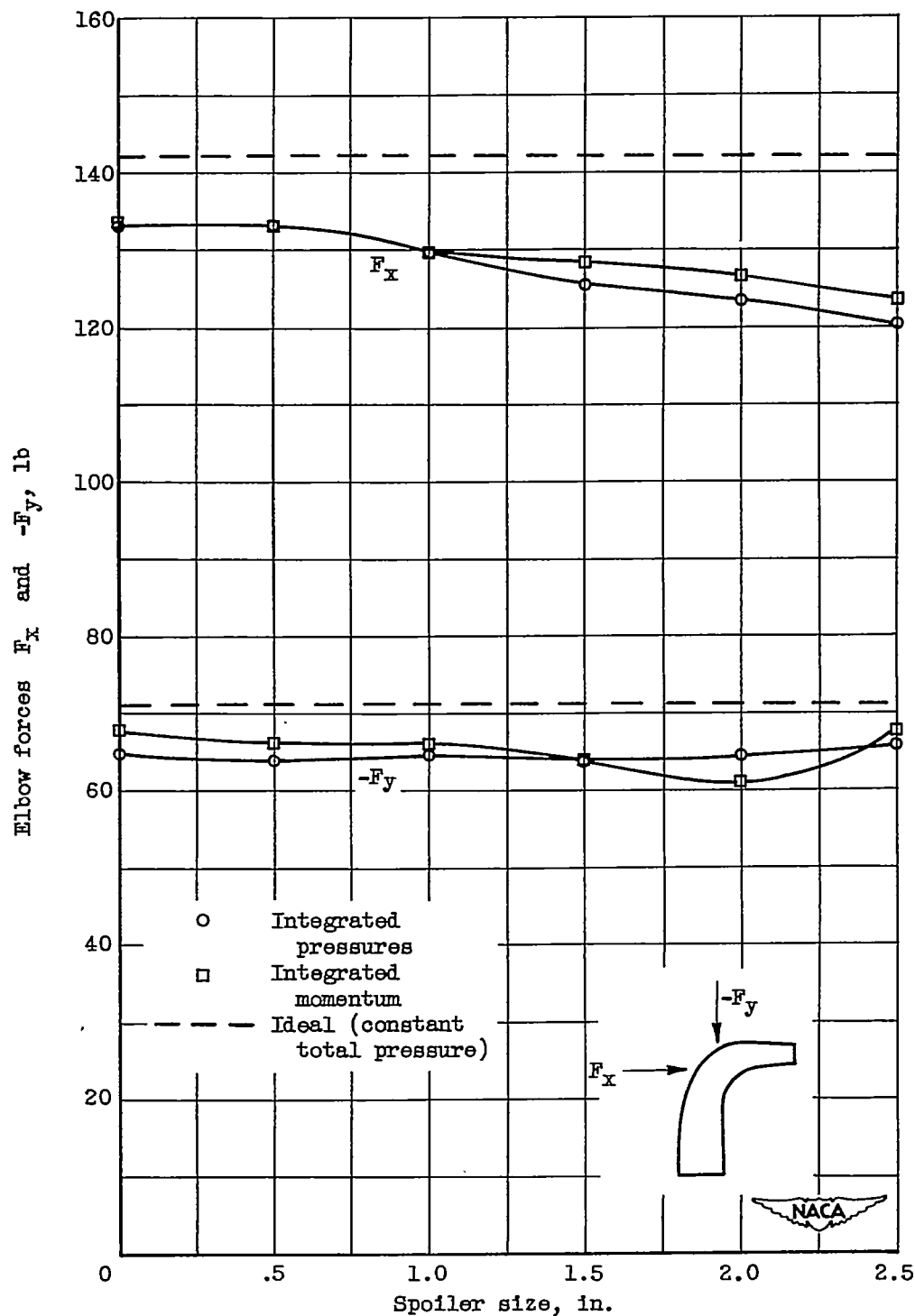


Figure 19. - Variation in x and y components of elbow force acting on fluid with spoiler size. Tank gage pressure ($p_T - p_a$), 20 inches of water.